# CHINA-AUSTRALIA CCUS INTEGRATED INTERNATIONAL COOPERATION DEMONSTRATION PROJECT

## Monitoring Technology for $CO_2$ Geological Sequestration in Ultra-Low Permeability Reservoir of Yanchang Petroleum

Shaanxi Yanchang Petroleum (Group) Co., Ltd.

March 2017

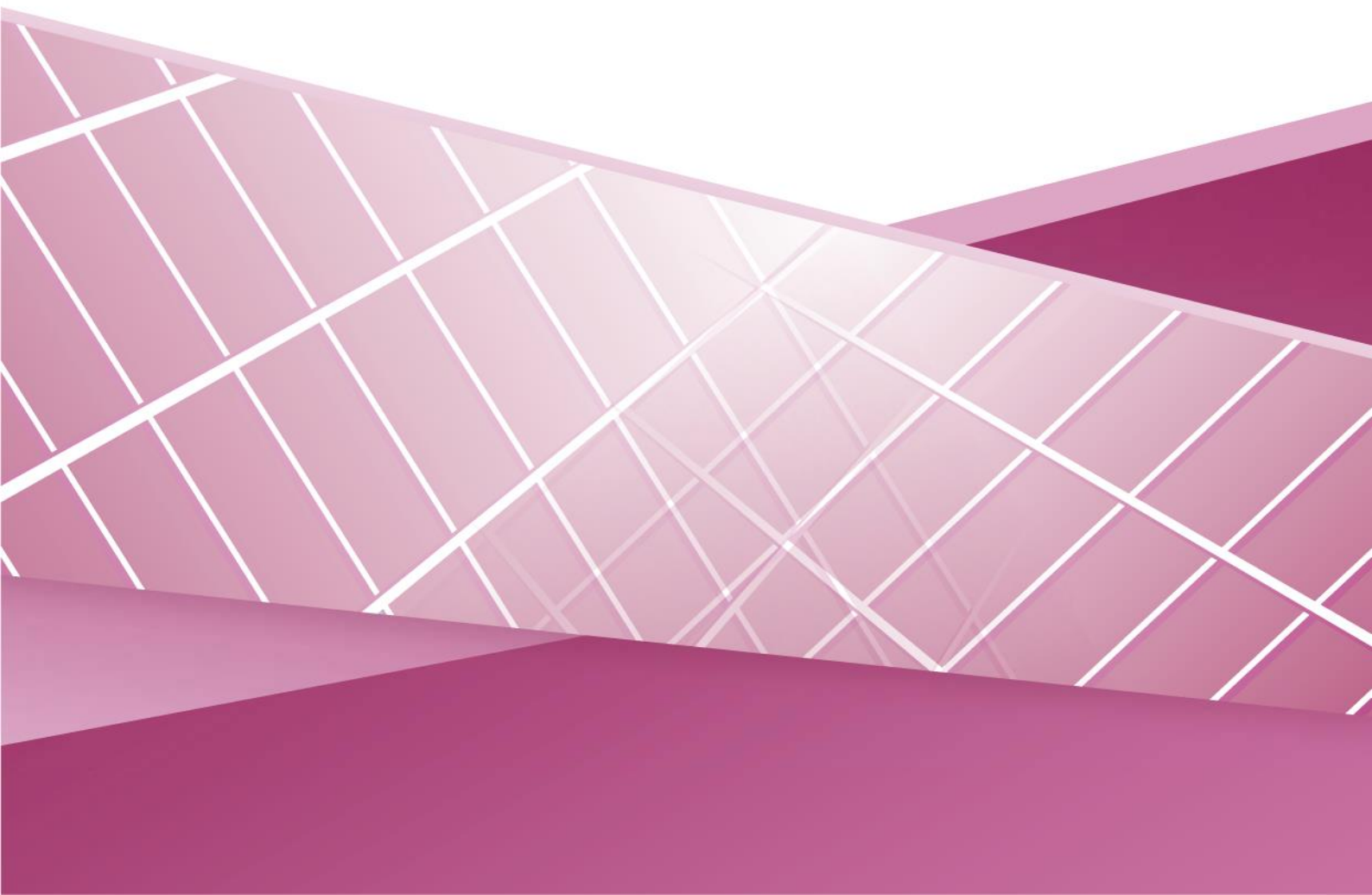

Prepared by:

- Wang Hong, Liang Kaiqiang
- Leading research institution: Research Institute of Yanchang Petroleum (Group) Co., Ltd.
- Jingbian Oil Production Plant of Yanchang Petroleum
- Wuqi Oil Production Plant of Yanchang Petroleum
- Research participants: Northwest University
- China University of Petroleum (Beijing)
- Sinopec Geophysical Corporation Zhongyuan Branch

# Table of contents

# 1 Introduction

Yanchang Petroleum has been engaging in carbon dioxide ($CO_2$) capture, utilisation and sequestration (CCUS) for a coal conversion project in northern Shaanxi Province since 2010. The pilot experiment for $CO_2$ flooding and sequestration (known as $CO_2$-EOR) was initially completed in the Jingbian and Wuqi counties, Shaanxi Province. By July 2015, Yanchang Petroleum had built the skid-mounted injection stations for $CO_2$-EOR to serve five well groups in Chang-6 Oil Reservoir of Qiaojiawa Block, Jingbian County, with the cumulative injection volume of 48,000 tonnes (t) liquefied $CO_2$. Yanchang also built the skid-mounted injection stations for $CO_2$-EOR to serve five well groups in Chang-4+5 Oil Reservoir of Yougou Block in Wuqi County, with a cumulative injection volume of 2,767.8t liquefied $CO_2$. Both injection projects are ongoing.

Safe and secure storage of $CO_2$ is the cornerstone of $CO_2$ geological sequestration (herein sequestration). After injection of $CO_2$ into the reservoir, the location and state of $CO_2$ migration in the reservoir needs to be determined. Additionally, the permanency and effectiveness of sequestration must be evaluated. To achieve this, monitoring and management procedures at the sites are put in place and include four focus areas:

1. $CO_2$ injection rate and pressure which can be effectively controlled by monitoring the injection wells
2. Location of the $CO_2$ plume, confirmed by monitoring the $CO_2$ distribution and migration in the subsurface
3. Risk of leakage arising from non-closure of abandoned wells, effectively avoided by well monitoring
4. Potential risks, detected by monitoring the local subsurface and surface environment

A comprehensive preliminary monitoring system is being completed against each of these focus areas at the Yanchang CCUS sites. This includes the planning and development of monitoring, measurement and verification (MMV) methods, as well as research and engineering development of MMV technologies in three stages:

1. Background data measurement before $CO_2$ injection, also known as baseline monitoring
2. $CO_2$ distribution during $CO_2$ injection, $CO_2$ leakage detection and well integrity monitoring
3. Calculation and verification of sequestration capacity after $CO_2$ injection and subsequent research of sequestration safety monitoring strategies.

Through strategic planning, research and development, the effectiveness of the sequestration operation at each of the stages can be improved. Also, improvements for monitoring and detection could potentially reduce the environmental and personal hazard caused by potential $CO_2$ leakage. The preliminary MMV program lays a solid foundation for risk management and decision-making processes at the Yanchang CCUS sites.

# 2 MMV technology status

The Global Status of CCS: 2016 shows that there are 38 large-scale CCS/CCUS projects in planning, construction and operation all over the world. This includes eight projects in China (Global CCS Institute, 2016). For all of these CCUS projects, a key goal is to ensure efficient sequestration through reliable and precise MMV technology. The recent focus on research into the technologies and techniques of monitoring, highlights the importance of MMV for a CCUS project to progress (Jenkins et al. 2015). Table 1 defines key monitoring methods used in CCS projects worldwide.

**Table 1. Important Monitoring Methods Used in Several CCS Projects.**

| Project Name | Key Monitoring Technologies |
|---|---|
| **Sleipner $CO_2$ Storage Project (Norway)** | $CO_2$ is currently being injected into the Utsira Sand at an injection rate around 1 million tonnes per annum (Mt/a) since 1996. Prior to, and during injection, $CO_2$ migration was regularly monitored by time-lapse seismic monitoring. Good seismic results of the $CO_2$ migration plume was achieved. |
| **SECARB Mississippi Test Site (USA)** | In 2008, 2,740 t of $CO_2$ was injected into the massive sandstone in the Tuscaloosa Formation, located close to the power plant. There was one injection well and one monitoring well. The monitoring methods were:<br>▪ wellhead and downhole pressure monitoring<br>▪ tracer injection<br>▪ vertical seismic profiling<br>▪ cement quality evaluation<br>▪ thermal decay time monitoring: a series of thermal decay time loggings to monitor if $CO_2$ escaped from the caprock<br>▪ shallow soil flux monitoring |
| **SECARB Cranfield Project (USA)** | From 2009-2015, over 5Mt of $CO_2$ was injected and monitored within the Tuscaloosa Formation, down dip from the mature Cranfield Oil Field. Highlighted technologies include:<br>In-zone and above-zone pressure surveillance<br>Electric resistivity tomography (ERT) showing daily changes in $CO_2$ saturation. |
| **Nagaoka $CO_2$ Storage Project (Japan)** | In 2003 until 2005, 10,400 t of $CO_2$ at an average injection rate of 20 – 40 t/d was injected into the Haizume Formation above the Nagaoka gas field. One injection well and three monitoring wells were drilled and underwent electrical logging and core analysis. Some of the monitoring methods used included:<br>▪ geophysical well logging<br>▪ elastic wave tomography<br>▪ cross-well tomography<br>▪ microtremor observation<br>▪ groundwater sampling |
| **In Salah $CO_2$ Storage Project (Algeria)** | From 2004 till 2011, 3.8Mt of $CO_2$ was injected into the main Krechba Sandstone. The most notable monitoring technology was the use of ASAR (Advanced Synthetic Aperture Radar) with a wavelength of 5.6cm on board the ESA ENVISAT satellite to measure surface displacement. |
| **Jilin Oil Field EOR Demonstration Project (China)** | In the EOR project of Jilin oilfield, tracer monitoring techniques provided important support to the successful implementation of the project. Tracers including HTO, sulfur-35 and indium-113 were used and assayed by a liquid scintillation analyser to produce the tracer production concentration curve. The permeability, equivalent thickness and swept volume of the main permeability channel between two wells were calculated by tracer interpretation software to get average permeability and other parameters. |
| **CCS demonstration project of China Shenhua Group** | For monitoring of the project, a control room was set up in the sequestration area to facilitate the real-time monitoring and timely adjustment of conditions and parameters (eg, $CO_2$ injection temperature, pressure, concentration and composition).<br>The project is injecting 100,000t/a and is undertaking: |

| | |
|---|---|
| | ▪ well logging monitoring (acoustic logging, natural gamma logging, sidewall coring)<br>▪ downhole formation water analysis<br>▪ temperature/ pressure monitoring techniques<br>▪ well tracer injection<br>▪ vertical seismic profiling<br>▪ 3D seismic<br>▪ ambient air quality monitoring<br>Porosity, permeability and saturation data were obtained by sample analysis. Reservoir capacity and $CO_2$ migration trends were forecast.<br>For air quality monitoring, five monitoring points were distributed in the capture area and the neighbouring residential area, 15,000m in the upwind/downwind direction of the sequestration area and 2,300m northwest of the capture area. $CO_2$, SO2, TSP, Pm10, NO2 and CO was monitored. The monitoring data provides basic data for monitoring during and after injection.<br>Before drilling of injection wells, 3D seismic monitoring was done and the full coverage was 54$km^2$. Five sets of data volumes were processed, including lithology (preserved amplitude), structure (pre-stack time migration, PSTM), separated offset stack (near, medium and far offsets). |

It is urgent for China to research and develop the monitoring technology applicable for sequestration, and design and establish a complete monitoring system and a leakage early-warning and treatment mechanism. China has accumulated data in oilfield sequestration projects and possesses mature seismic, tracer, well and logging monitoring technologies. In view of available monitoring technologies in China, well, logging and seismic monitoring technologies will receive more attention and application going forward. However, there are a number of other monitoring technologies available and their application to projects and outcomes differ. This makes it necessary to analyse various applications to China's CCS projects. The most economical and effective monitoring Chinese project technologies should be the focus of China's CCS community. It is anticipated that with further research of MMV technologies and the development of MMV projects, certain monitoring technologies like ERT, satellite spectral imaging and on-board infrared spectrum analysis may be applied to China gradually. This will lead to greater diversity of monitoring technologies in China.

# 3 Jingbian and Wuqi: Geology and geological modelling

Geological modelling and numerical simulations are regarded as a key part of an MMV program. A model of a sequestration site supports risk management by identifying project uncertainties and forms the basis of $CO_2$ plume migration. For the Jingbian and Wuqi sequestration reservoirs, modelling has three major purposes.

The first purpose is to seek a favourable reservoir suitable for sequestration.

The second purpose is to image the heterogeneity that may affect the characteristics of $CO_2$ fluid migration, accumulation and seepage in the reservoir. This will be achieved by modelling the heterogeneity through quantitative description of the spatial distribution of porosity, permeability and saturation in the reservoir, and provide the model foundation for numerical simulation.

The third purpose is to quantitatively describe the characteristics of spatial distribution of caprock displacement pressure and the spatial configuration relationship of reservoir cap, and evaluate the sealing property of the caprock. After optimisation and comparison of modelling methods, geological models of the storage complex are created by integrating deterministic modelling with stochastic modelling. This requires a deep understanding of the site's geology including the constraint and control of the sedimentary facies and sand body distribution trend, as well as requiring sufficient data about the sequestration conditions.

## 3.1 Geology of Qiaojiawa block and 3D geological modelling

Jingbian Oilfield is located in the mid-south of Jingbian County, in the mid-east of the North Shaanxi Slope of the Ordos Basin. The Qiaojiawa exploration area is located in the north of Jingbian Oilfield. The regional structure of this area is a monoclinal structure, high in the east and low in the west characterised by a simple internal, gentle structure with an absence of clear faults and tectonically stable. The primary target is the Triassic-aged Upper Yanchang Formation, one of the most prolific oil producing formations in the basin (Shaanxi Yanchang Petroleum, 2015). It is also characterised as a low porosity, low to ultra-low permeability formation with low reservoir pressure and high heterogeneity. The lithofacies of the Yanchang Formation is described as a fluvial environment, with reservoirs forming in distributary channels and caprock lithofacies defined as flood plain.

The main oil-bearing formation of Jingbian Oilfield is Chang-6 oil reservoir group which sits within the Yanchang Formation. This reservoir group is further split into three oil reservoirs, Chang-63, Chang-62 and Chang-61.Chang-62 is the major oil reservoir in the Qiaojiawa area. The effective geological capacity of the Qiaojiawa exploration area are 339.95×104 t based on the results of the geological modelling using the capacity calculation method of the CSLF (2007) calculation.

**Figure 1. Generalised stratigraphic column of Triassic Ordos Basin.**

| Age | | Formation | Oil Members | Layers | |
|---|---|---|---|---|---|
| Triassic | Upper | Yanchang | Chang1 | | |
| | | | Chang2 | | |
| | | | Chang3 | | |
| | | | Chang4+5<br>Jingbian caprock<br>Wuqi reservoir/caprock | | |
| | | | Chang6<br>Jingbian reservoir | $Chang6_1$ | |
| | | | | $Chang6_2$ | $Chang6_2^{1-3}$ |
| | | | | $Chang6_3$ | |
| | | | Chang7 | | |
| | Middle | | Chang8 | | |
| | | | Chang9 | | |
| | | | Chang10 | | |

### 3.1.1 Structural model

In the target interval, there are no large faults and only a few natural fractures are developed, with low topographic relief. Considering these geological features, it is not necessary to create a fault model for Jingbian. The main task is to establish the 3D distribution trend of the top horizon of each formation. The structural model of each formation is successive and presents the general trend of high in the east and low in the west. In addition, some nearly E-W nose-shaped uplifts exist in local parts (See Figure 1). The fine structure model is the framework model for additional geological property modelling.

**Figure 2. Structural model of Qiaojiawa block of Jingbian Oilfield.**

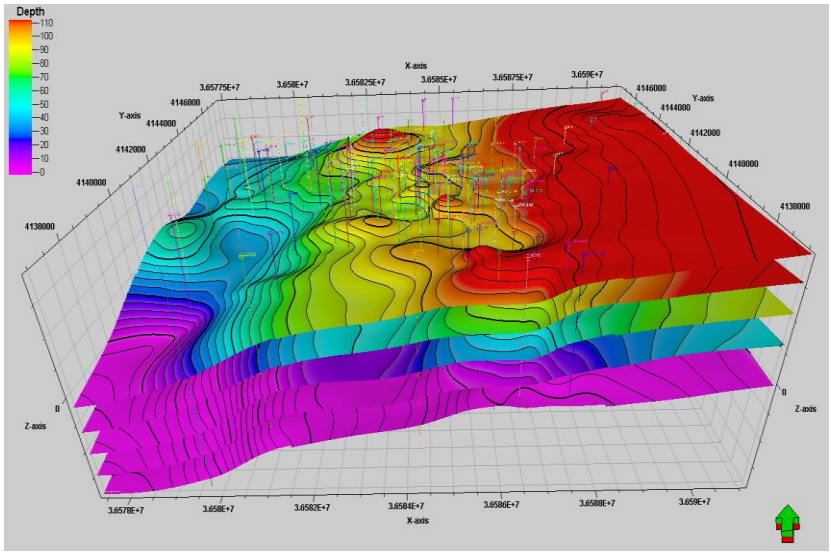

### 3.1.2 Lithofacies modelling

Controlled by the regional fluvial sedimentary setting, the lithofacies model is created first. This is achieved through digitally mapping the sand distribution on isopach maps which is matched to core and well logging analysis to constrain the boundaries and distribution of lithologies in the model. Well control is good with well spacing in the Qiaojiawa Block around 200m-300m. According to the core and well logging data interpretation there are four distinct sandstone units: poor oil layer (oil layer but no production), oil-water layer (oil saturation more than 40 per cent; main oil production layer), water with oil layer (oil saturation less than 40 per cent, not the oil production layer) and water layer (water saturation is more than 98 per cent). These sandstone units were deposited in distributary channels. The ‘dry layer’ unit is classified as argillaceous mudstone deposited in a flood plain environment. After comparison with geological analysis results, the lithofacies model, which is the best fit for geological research results was created and the results are shown in Figure 2.

**Figure 3. Yanchang Formation lithofacies model, Qiaojiawa Block of Jingbian Oilfield after applying trend-surface (reservoir (yellow), non-reservoir (grey). a. Chang-4+5. b. Chang-62.**

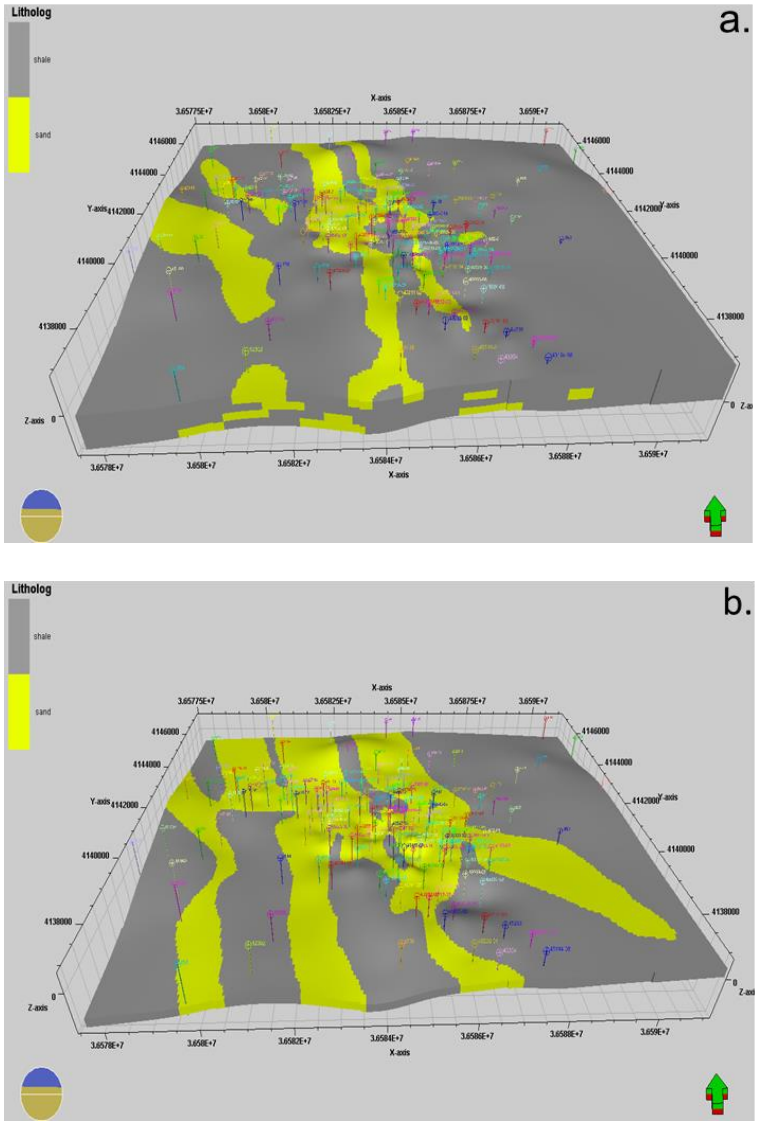

### 3.1.3 Reservoir property modelling and characterisation

Stochastic reservoir property modelling is used to establish the distribution model of porosity, permeability and saturation parameters. Depending on the reservoir property continuity and normal distribution characteristics, the model's reservoir properties are populated using sequential Gaussian simulation, which is controlled and constrained by the lithofacies model. The results can be seen in figures 3-5.

- Porosity model: From the porosity model (Figure 3) the distribution of the porosity of each formation is strictly controlled by sedimentary facies. The distributary channel (yellow in Figure 2) is a thick sandstone, comprising good sorting and rounding and high in porosity, whilst the argillaceous mudstone was deposited as a flood plain (grey in Figure 2) is low in porosity. As expected, the general porosity distribution of the regional caprock Chang-4+5 is inferior to Chang-6. The $CO_2$ injection target lithofacies is primarily Chang-6 sandstone. The major oil reservoir Chang-62, is the main sand body member and is located in the middle of the Chang-6 formation with a thin shale member developed on the top of this formation. For this reason the porosity model of Chang-62 (Figure 3a) has a similar lower value to the overlying Chang-4+5 shale member, but the connected wells' profile and grid map (Figure 3b) better reflects the member with higher porosity values in the middle of this formation.

**Figure 4. Porosity Model of Reservoir and Caprock of the Yanchang Formation, Qiaojiawa block of Jingbian Oilfield. a. Porosity model of Chang-62 surface. b. Porosity fence diagram. Scale bar is porosity (Φ) ranging from red (15%) to green (1%).**

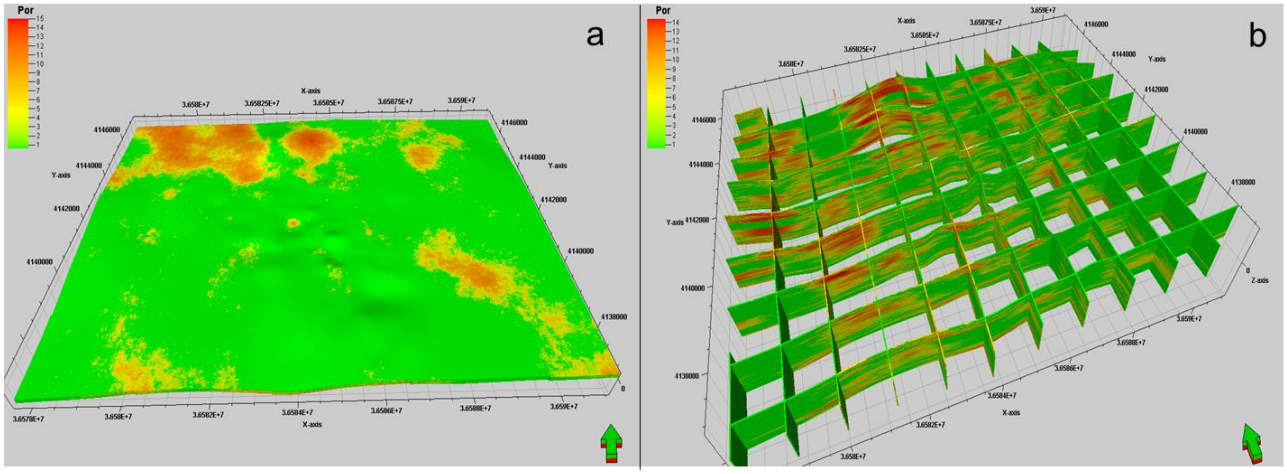


- Permeability model: There is good correlation between porosity and permeability in the Chang-6 sandstones in Jingbian Oilfield, so the porosity model was used as the constraint when creating the permeability model. From the permeability model, the permeability is controlled by the lithofacies, but it is more discrete compared with porosity distribution. The permeability distribution of the Chang-4+5 caprock is much lower to the permeability of Chang-6. Chang-62 gives the best permeability distribution (See Figure 4).

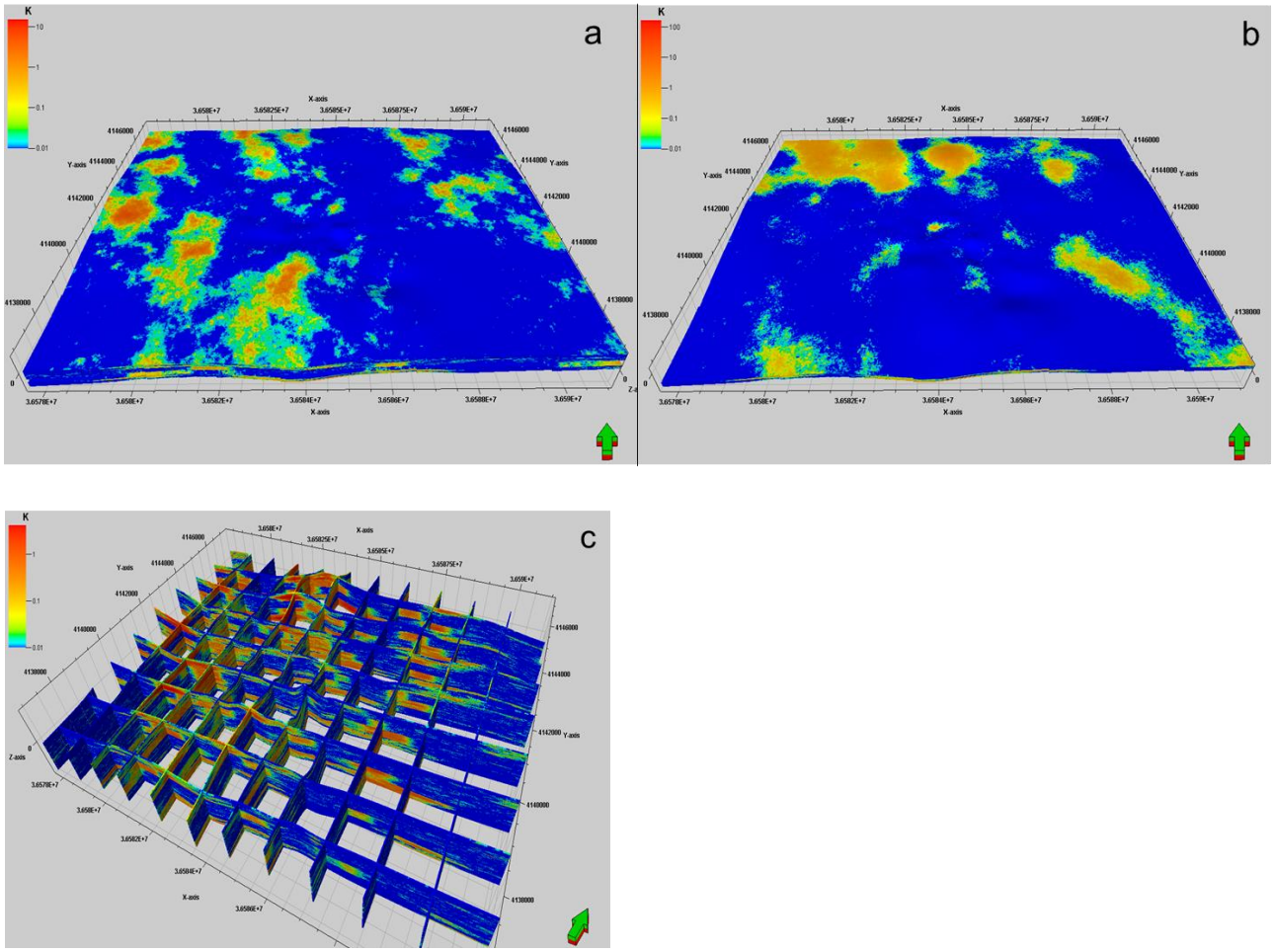


**Figure 5. Permeability model of the Yanchang Formation, Qiaojiawa block of Jingbian Oilfield. a. Chang-4+5. b. Chang-62. c. Permeability fence diagram. Scale bar is permeability (mD) ranging from red (100) to blue (0.01).**

- By analysing the lithology-log relation, the oil saturation of the reservoir in the research area could be measured. Based on the data, the oil saturation model in the main sequestration reservoir was created (See Figure 5). This models shows that oil saturation distribution of the Chang-4+5 is inferior to Chang-6. This is consistent with the Chang-4+5 being a regional caprock that cannot produce oil. As a major oil-producing horizon in the research area, Chang-62 has the best oil-bearing property with the oil saturation above 35 per cent.
- The distribution range of displacement pressure of Chang-4+5 caprock is much higher than the Chang-6 reservoir. The displacement pressure distribution is steady and uniform in the whole area except several sporadic zones with lower value. The distribution range of displacement pressure of the Chang-6 reservoir is inferior to Chang-4+5 (Figure 6), but the general distribution is relatively uniform. For both Chang-61 and Chang-62 pressure distribution is low in the north and high in the south. Generally, Chang-4+5 is an ideal regional caprock, but Chang-6 can also block the oil ($CO_2$) fluid in the reservoir to certain extent because of intraformational mudstones (See Figure 6).

**Figure 6. Figure 6. Oil saturation model of the Yanchang Formation, Qiaojiawa Block of Jingbian Oilfield. a. Chang-4+51. b. Chang-62. c. Oil saturation fence diagram Scale bar is oil saturation (%) ranging from red (60%) to purple (5%).**

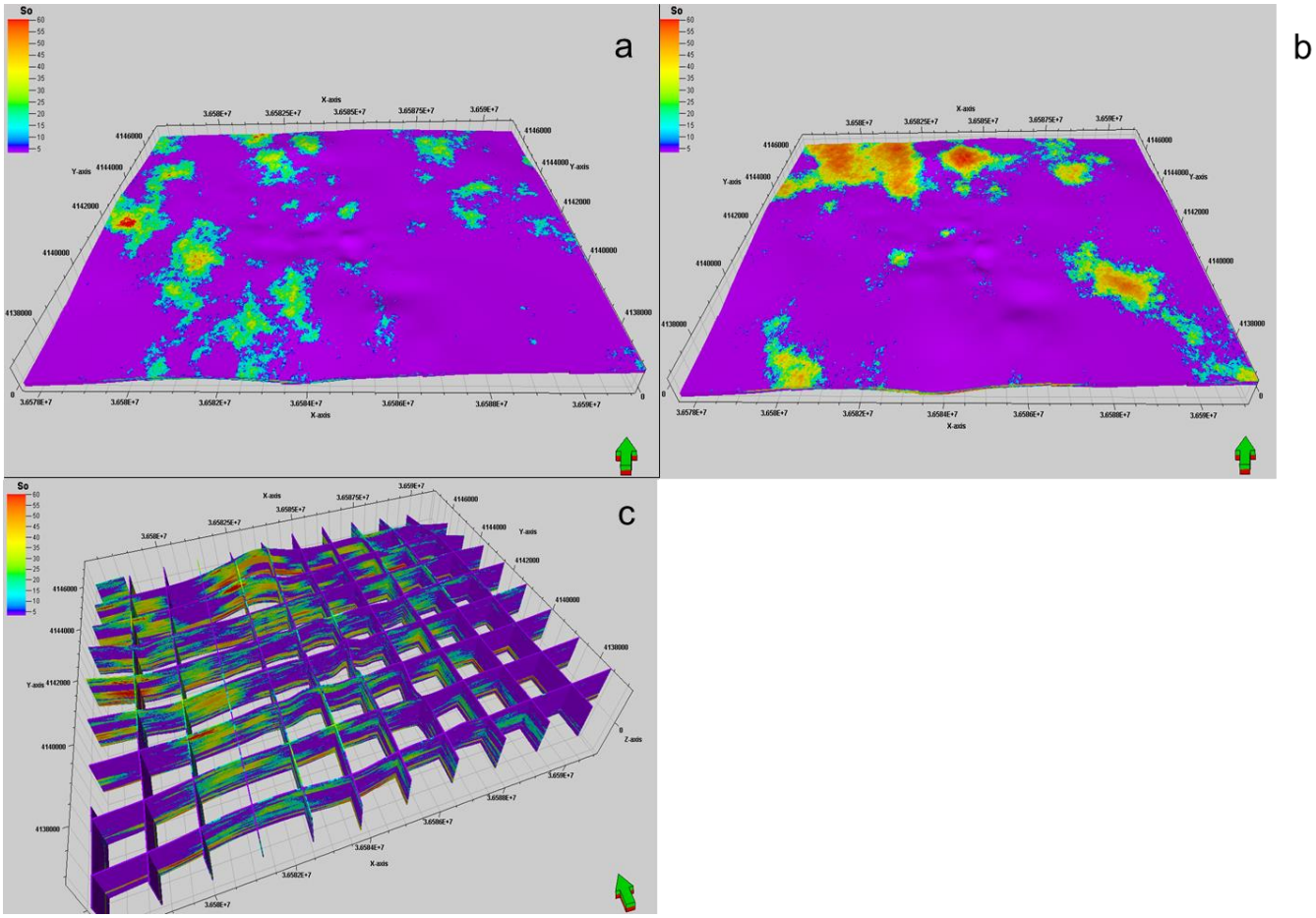

**Figure 7.Displacement pressure model of the Yanchang Formation, Qiaojiawa Block of Jingbian Oilfield. a. Chang-4+51. b. Chang 4+52. c. Displacement pressure fence diagram. Scale bar is displacement pressure (MPa) ranging from red (8) to purple (0).**

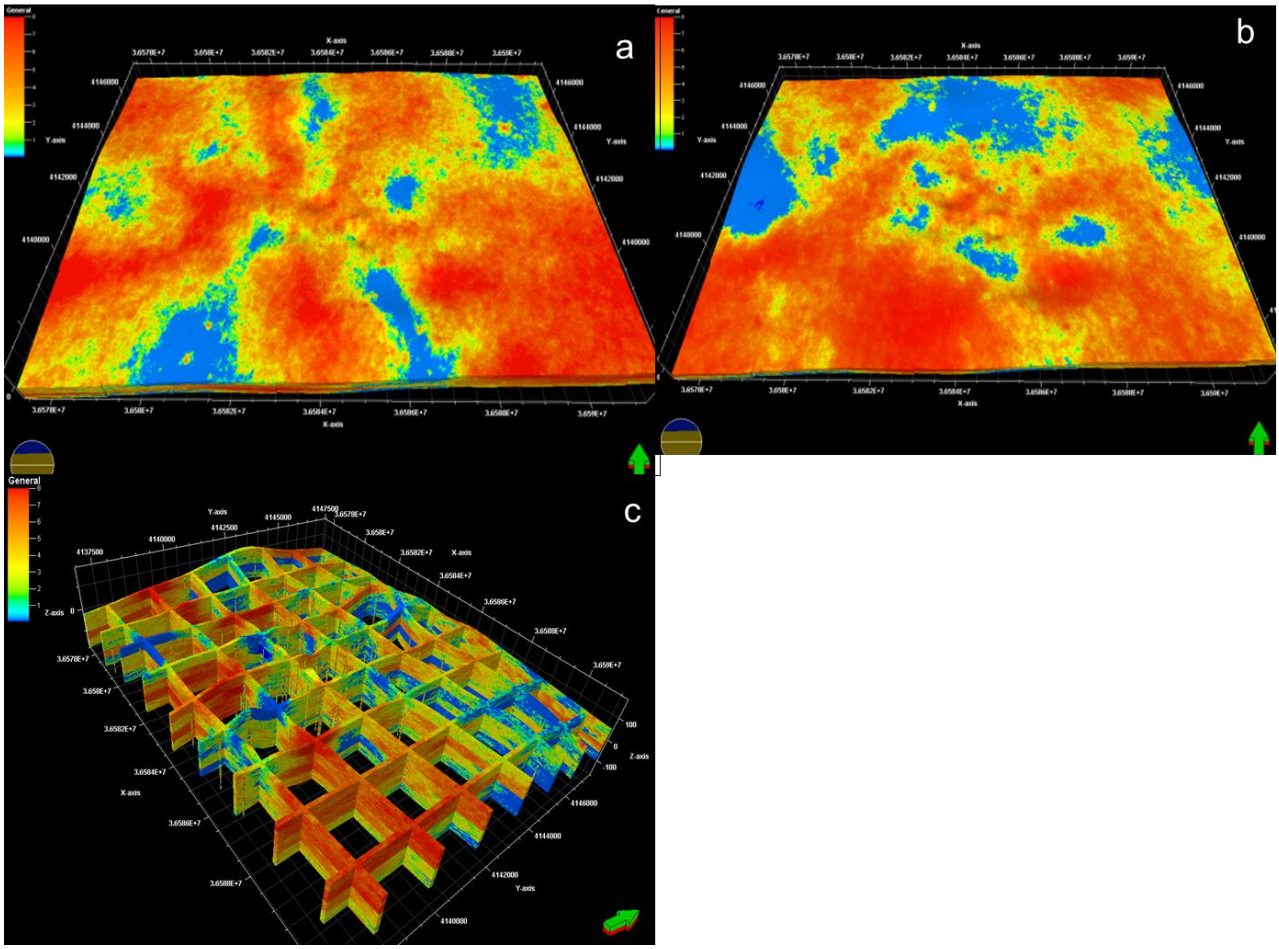


## 3.2 Geology of Yougou block and 3D geological modelling

Wuqi Oilfield is located in Baibao Township, Wuqi County, Shaanxi Province, within the mid-south of the North Shaanxi Slope of the Ordos Basin. The Yougou exploration area is located in the centre of Wuqi Oilfield. The target interval Chang-4+51 undulates and forms a large nose-shaped uplift. This exploration area is characterised by a seismically stable simple structure, with an absence of clear faults... In contrast to the Jingbian Oilfield which is caprock, the Chang-4+51 is an oil and gas reservoir in the Triassic Yanchang Formation of Yougou Block. The oil sandstone reservoir was deposited in a delta-front distributary channel and oil accumulated within a nose-shaped uplift. As a major oil reservoir of this area, Chang-4+51 has an oil-bearing area of 13.85km2 and oil reserves of 565.39×104t.

### 3.2.1 Structural model

**Figure 8. Structural model of the Yougou Block in Wuqi Oilfield showing the upper most surface of Chang-4+51. a. wells. b. without wells.**

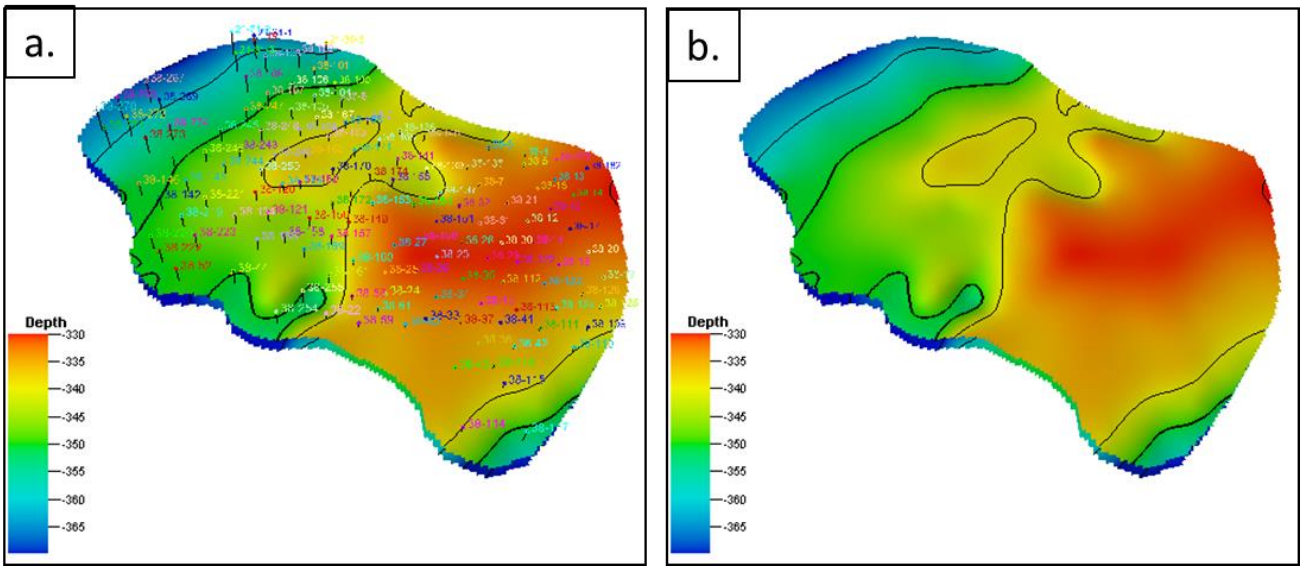


The 3D structural model of Yougou Block in Wuqi Oilfield was constructed using a layered superposition method created by the deterministic modelling. The spatial extent and depth of each layer was derived from well data. Firstly from well data, the top and bottom layer of each formation was defined and then by interpolation, a surface was created. Each subsequent layer was superimposed from these surfaces (See Figure 7).

### 3.2.2 Lithofacies modelling

**Figure 9. Lithofacies Distribution Model of Chang-4+51 of Yougou block in Wuqi oilfield. The red line is cross-well profile of Figure 9 and the blue line is Figure 10.**

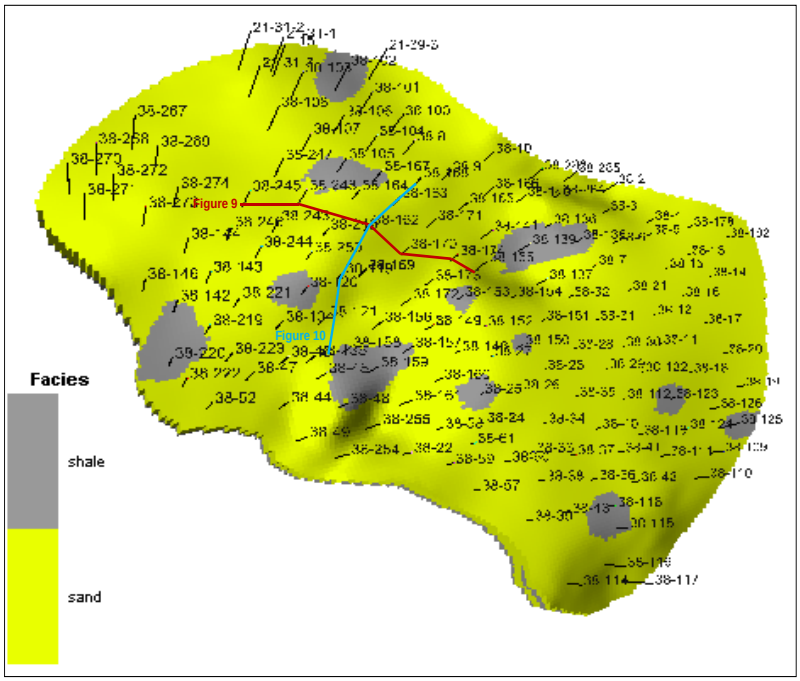


The classification of the lithofacies in the model is based on the comprehensive logging interpretation results. According to the interpretation, the poor oil layer (oil layer but no production), oil-water layer (oil saturation more than 40 per cent - and the main oil production layer), water with oil layer (oil saturation less than 40 per cent, not the oil production layer) and water layer (water saturation is more than 98 per cent) are classified as sandstone Lithofacies. Distribution was populated in the model by the indicator Kriging method. The lithofacies models created are shown in Figures 8 to 10.

**Figure 10. Cross-well Profile showing the lithofacies in the west of test area (E-W) in the Yougou Block in Wuqi oilfield.**

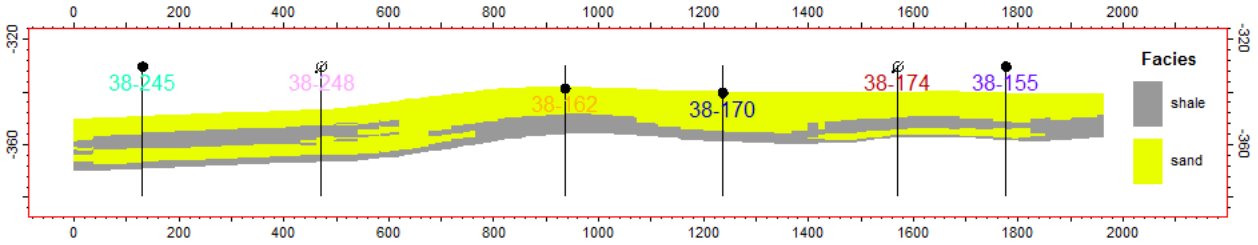

**Figure 11.Cross-well Profile showing the lithofacies in the west of test area (S-N) in the Yougou block in Wuqi oilfield.**

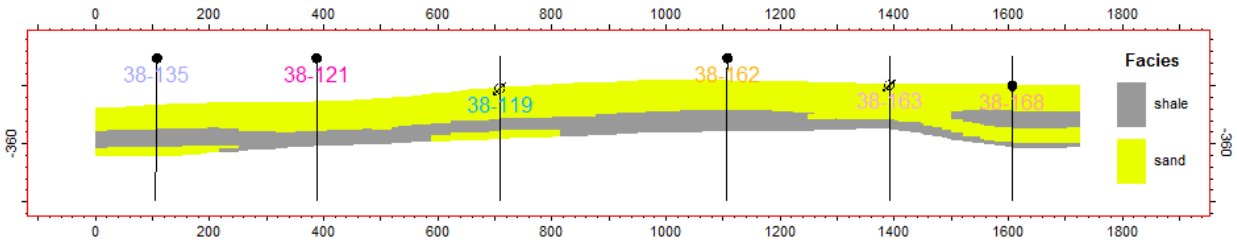


### 3.2.3 Reservoir property modelling and characterisation

As expected, facies controls the distribution of physical parameters in this model. The facies-restrained stochastic modelling method fits the geological parameters (porosity and permeability). The $CO_2$ test area in Yougou Block is a low-permeability, oil reservoir with small-permeability range (0.01md-4.0mD) and non-uniform distribution of porosity and permeability. The well row spacing is between 220m and 350m. The property model was created by the sequential Gaussian and inverse distance square (IDS) weighted algorithm and the facies-constrained interpolation method.

- Porosity 3D model: The porosity model of Chang-4+51 was created according to the porosity of the oil reservoir obtained by logging interpretation. As the porosity of shale facies is assigned to 0.04, the 3D property field probability distribution is slightly different from the interpretation of logging data.

**Figure 12. 3D schematic diagram of porosity of Chang-4+51 in the Yougou Block in Wuqi oilfield. Scale bar is porosity (Φ) ranging from red (25%) to blue (1%).**

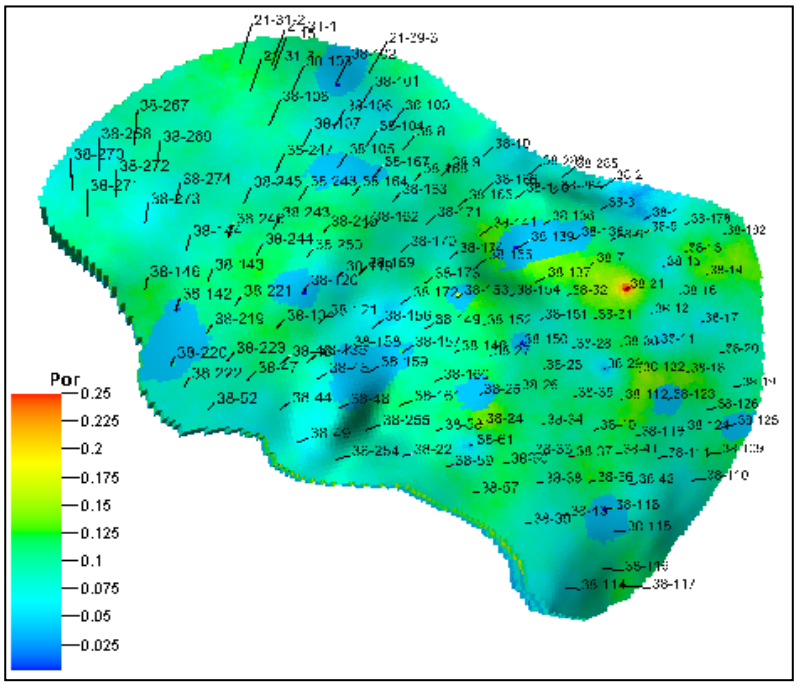

**Figure 13. Cross-well profile showing the porosity in the west of oil reservoir (E-W); (see figure 8 for well profile location). Scale bar is porosity (Φ) ranging from red (25%) to blue (1%).**

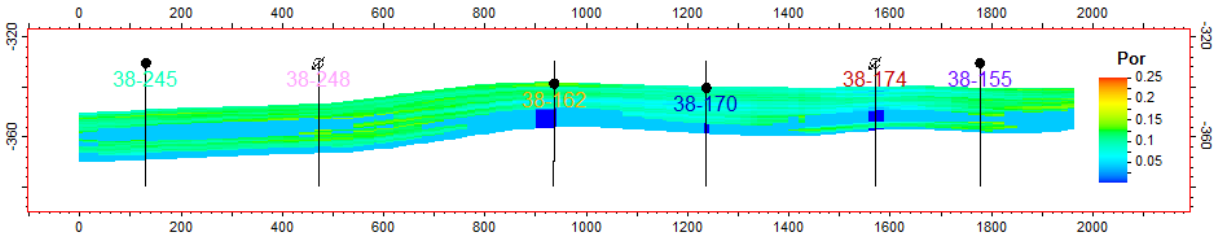


**Figure 14. Cross-well profile showing the porosity in the east of oil reservoir (S-N); (see figure 8 for well profile location). Scale bar is porosity (Φ) ranging from red (25%) to blue (1%).**

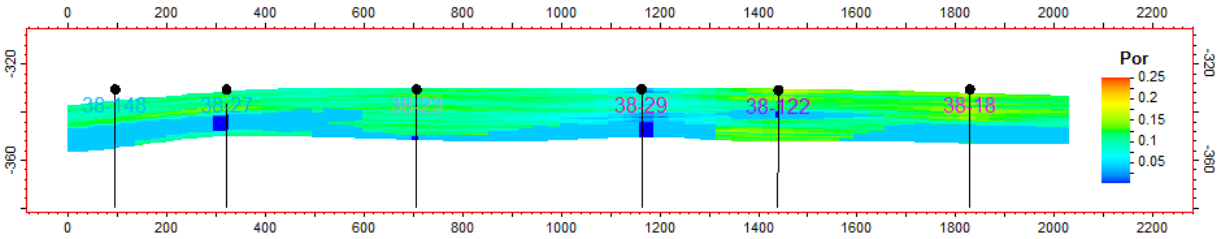


- Permeability 3D model: the porosity model of the Chang-4+51 sub-layer was created according to the porosity of the oil reservoir as obtained from logging interpretation. As the permeability of shale facies is assigned to 0.001, the 3D property field probability distribution is slightly different from the logging data. Figures 14 to 16 are 3D schematic diagram and cross-well profiles of the permeability model.

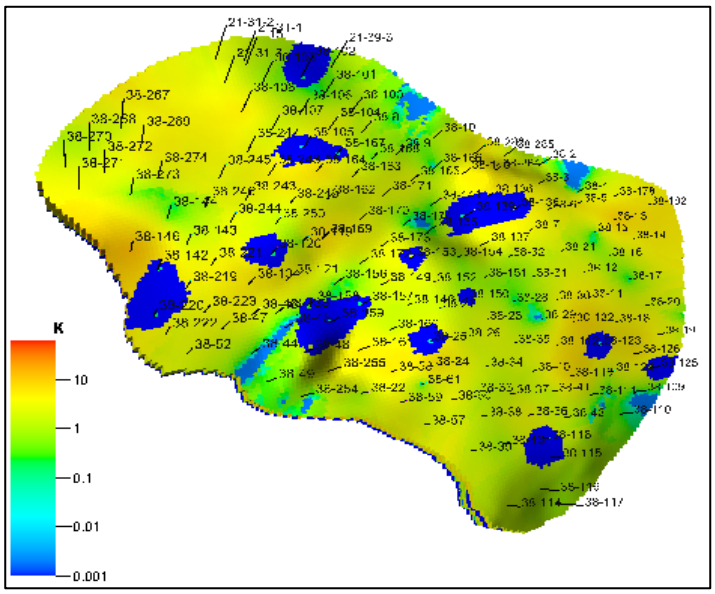


**Figure 15. 3D Schematic Diagram of Permeability (K, millidarcy) of Chang-4+51 in the Yougou Block in Wuqi Oilfield. Scale bar is permeability (mD) ranging from red (100) to blue (0.01).**

**Figure 16. Cross-well Profile Showing the Permeability (K, millidarcy) in the West of Oil Reservoir (E-W) Scale bar is permeability (mD) ranging from red (100) to blue (0.01).**

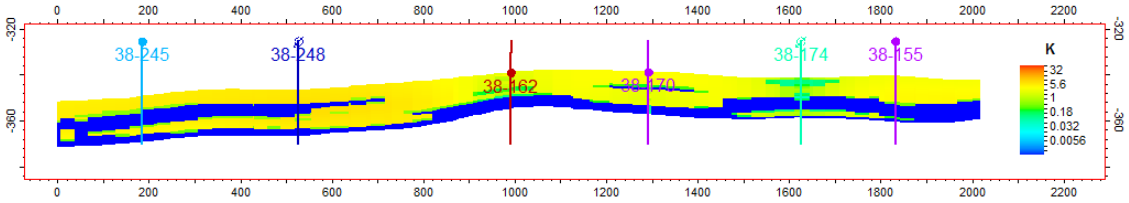


**Figure 17. Cross-well Profile Showing the Permeability (K, millidarcy) in the East of Oil Reservoir (S-N). Scale bar is permeability (mD) ranging from red (100) to blue (0.01).**

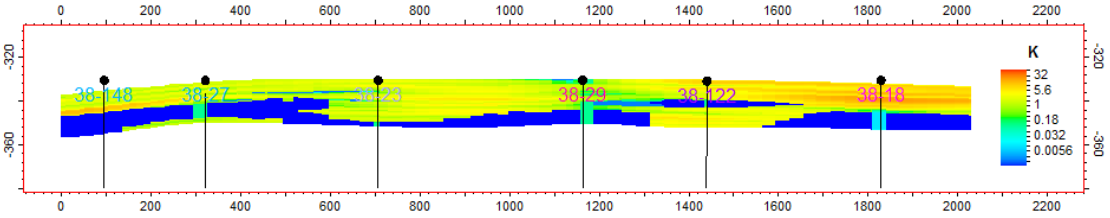


- Net to Gross (N/G) 3D model: Depending on the single-well effective thickness, N/G was entered into the model as a property. Figures 17 to 30 are 3D schematic diagram and cross-well profiles of the permeability model.

**Figure 18. 3D Schematic Diagram of N/G of Chang-4+51 in the Yougou Block in Wuqi Oilfield; (N/G units are expressed as a fraction, 1 is 100% sand).**

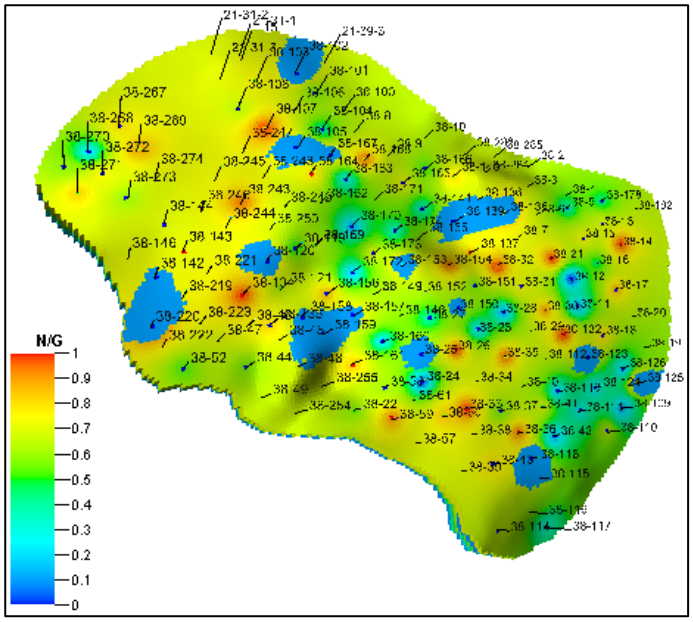

**Figure 19. Cross-well Profile Showing the NTG in the West of Oil Reservoir (E-W). (N/G units are expressed as a fraction, 1 is 100% sand).**

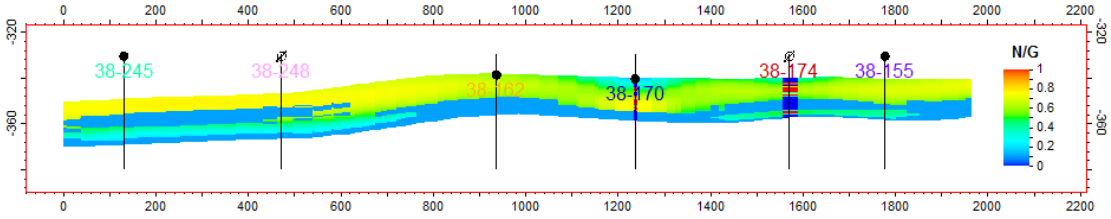


**Figure 20. Cross-well Profile Showing the NTG in the East of Oil Reservoir (S-N). (N/G units are expressed as a fraction, 1 is 100% sand).**

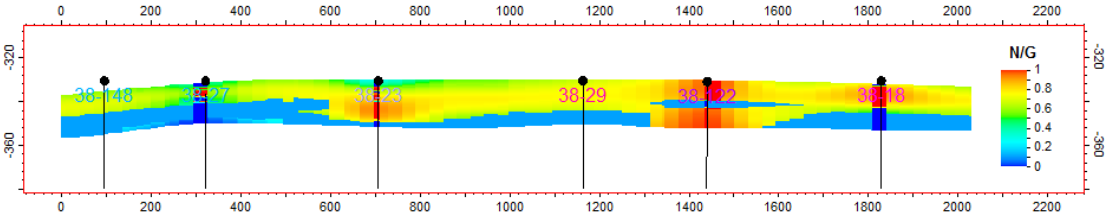

# 4 Downhole monitoring

## 4.1 Overview of well integrity

For the Yanchang CCUS Project, well integrity has been determined as the largest risk factor of leakage. Active wells are usually completed with steel casings and liners and the outer rings are filled with cement to prevent the leakage between casings and formation rocks. Abandoned wells are often sealed by cement for the purpose of stopping the vertical migration of liquid. Several potential leakage paths may exist along cased or abandoned wells, as shown in Figure 21.The leakage paths include:

- zone between cement and outer wall of casing (a)
- zone between cement and inner wall of casing (b)
- cement plug (c)
- casing wear (eg, rust) (d)
- cement wear(cement seam) in circular pore (e)
- zone between formation and cement (f)

**Figure 21. Possible leakage paths in abandoned well (Celia et al. 2005).**

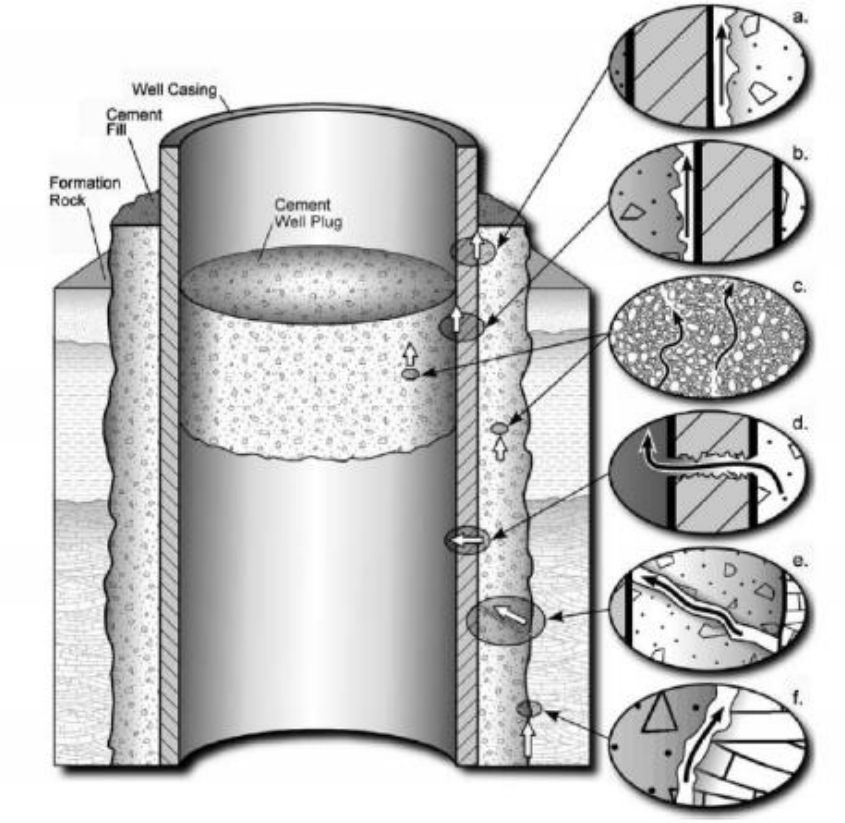

For injection wells where $CO_2$ exists, the exposure of well components to $CO_2$ may induce the corrosion of these components. The casings of production wells and the components of the casings of production wells under filters are usually corroded. Corrosion-resistant high-alloy chromium-containing steel can be selected to suppress corrosion. If carbon steel casing is used, corrosion can also be suppressed by injecting an inhibitor.

## 4.2 Well integrity index monitoring method

The Yanchang Projects will employ numerous well integrity monitoring indexes including string strength, corrosion rate, cement condition, leakage rate and thread tightness.

### 4.2.1 Residual wall thickness

The main method used by the petroleum industry to measure the residual wall thickness of casing is acoustic imaging logging. The main tool is a rotary ultrasonic transducer which is used for circular scanning and the collection of echo signals. Acoustic logging records the acoustic propagation time and determines the residual wall thickness of casing from echo time.

Basic steps: Assuming that the number of propagation times collected in one scan is N, the value of N echo times is recorded when the unworn casing is calibrated; after the target well is scanned once at certain depth, the value of N echo times obtained is recorded. The casing wall thickness reduction at the target depth of this well is recorded.

$$\bar{T}_c(d_c)=\sum_{i=1}^{N} T_c(i, d_c) / N \quad (2\text{-}2\text{-}1)$$

$$\Delta T(d)=\max|T_c(i, d)-\bar{T}_c(d_c)|v_s \quad (1)$$

Where: $T_c(i, d_c)$ ——$i^{th}$ echo time at site calibration, s;

$\bar{T}_c(d_c)$ —— Standard echo time calibrated on site, s;

$\Delta T(d)$ ——Wall thickness reduction at actual well depth (d), mm;

$v_s$ ——Acoustic velocity in steel, mm/s.

### 4.2.2 Corrosion rate monitoring

The corrosion coupon method is adopted for monitoring the corrosion rate in this project. After weighing a coupon (a small piece of material composed of the same material as the downhole tubing) and recording its weight, it is lowered down the well. Systematically, the coupon is removed for cleaning and weighing. When compared to the original coupon's weight and thickness, the corrosion rate can be calculated. The cleaning and measurement process is detailed below:

1. Take the corrosion coupon out of the hole, take a picture to record its original status, cover the surface with Vaseline, and wrap it with plastic film quickly to avoid oxidation due to exposure to the air.
2. Clean the coupon with petroleum ether to remove oil stains.
3. Wash the surface with clean water, and use a stiff brush to pick out the loose material on the surface of the corrosion coupon.

4. Suck dry the washed corrosion coupon with a filter paper. Soak the coupon in the diluted hydrochloricacid (10 per cent ~15 per cent) solution containing corrosion inhibitor (HexamethyleneTetramine, HMT) and continue to pick out the corrosion product.
5. Wash the coupon with tap water and suck it dry with a filter paper. Neutralise it with sodium hydroxide solution (the soaking time of the coupon shall not exceed 1min). After neutralisation, wash it with tap water again.
6. After washing the coupon to the required level, suck it dry with a filter paper. Then, soak it into absolute ethyl alcohol for 5min.
7. Suck it dry with a filter paper. Put it into a dryer. 24~48h later, weigh the coupon.
8. Based on the weight of the processed coupon, calculate the average corrosion rate according to the following formula:

$$V=3650M/(S\cdot t\cdot d) \tag{2}$$

Where: V—Corrosion rate, mm/a;

M——Coupon weight loss, g;

S——Exposed area of coupon, cm2;

t——Test duration, d;

d——Coupon density, g/cm3.

### 4.2.3 Cement condition monitoring

An acoustic amplitude logging tool is used to detect the condition of a cement ring. The measured curve value decreases with the increase of well cementing quality. Currently, the ratio of test-point acoustic amplitude to free casing scale value is regarded as a reference, namely:

$$\mu_{cbl}(d)=E_d/E_{d0}\times 100\% \tag{3}$$

Where: $\mu_{cbl}(d)$ ——Acoustic amplitude ratio, %;

$E_d$ ——Acoustic amplitude logging value at well depth (d), mV;

$E_{d0}$ ——Acoustic amplitude logging value of free casing, mV.

### 4.2.4 Leakage rate monitoring

If the pressure in the annulus (abnormal pressure in the annular can indicate leak or malfunction) of the production well is less than reserved pressure of 5MPa, it implies that there is almost no risk with annular pressure (see Figure 1). If this is the case, only routine monitoring is required in the operation area. If the annular pressure is above the completed-well reserved pressure (above 5MPa) but below the maximum allowable annular pressure range, it can be considered that there is some risk with annular pressure. In this

situation, diagnosis, test and analysis is required. When this occurs, it will be necessary to locate the cause of annular pressure, which could include the use of wireless pressure sensors to monitor oil pressure, oil-string casing pressure, intermediate casing pressure and surface casing pressure in real time. Monitoring data will be fed back by wireless transmission. The minimum leakage rate is required to be 0.42m3/min (gas) and 0.40L/min (liquid) (refer to APIRP14B standard).

### 4.2.5 Thread tightness monitoring

The thread tightness monitoring technique uses a helium-nitrogen mixture. The common mix ratio is 1:7 (helium: nitrogen), with helium used as search gas. Its molecular diameter is very small (smaller than $CO_2$ and methane so smaller leaks can be detected). It can leak into the sealing thread, but is not corrosive to the well casing. It is a non-poisonous, safe and inert gas. Nitrogen is used as the carrying gas and similarly, is not corrosive to casing, and is a cheap, non-poisonous, safe and inactive gas. For molecular permeability of different gases, see Table 2.

**Table 2. Permeability of different media (Compared with Helium at 25.5℃).**

| Gas | Hydrogen | Helium | Steam | Neon | Nitrogen | Air | Argon |
|---|---|---|---|---|---|---|---|
| **Molecular weight** | 2 | 4 | 18 | 10 | 28 | 29 | 40 |
| **Molecular permeability/mD** | 1.41 | 1 | 0.47 | 0.45 | 0.37 | 0.37 | 0.32 |

Air-tightness monitoring equipment: The air-tightness test equipment mainly consists of helium molecule detector, clamp, console, energy accumulator and power mechanism. The composition and working principle of air-tightness monitoring equipment are shown in Figure 23.

**Figure 22. Composition of air-tightness monitoring equipment (Jinan Simingte Company, China).**

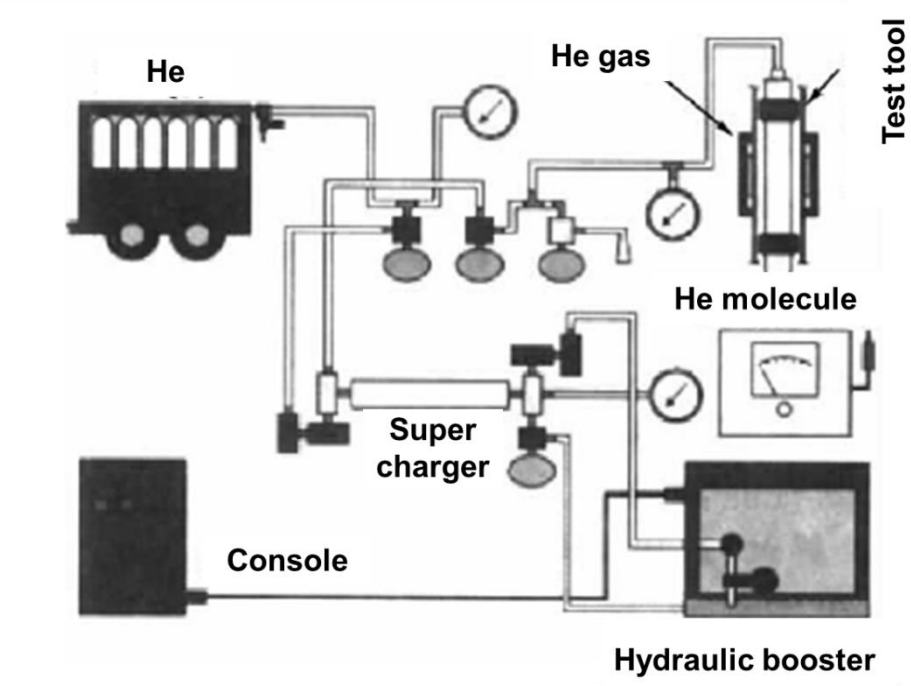

### 4.2.6 Pressure monitoring

Pressure monitoring is a simple method to understand if $CO_2$ leaks from the well shaft. The emphasis is on assessing the absolute annular pressure and pressure rise rate of the production well. If the absolute annular pressure is larger than 80 per cent of Maximum Allowable Working Pressure (MAWOP) and the pressure quickly restores and rises to the level before repeated pressure relief, it proves the total failure of production well integrity. If not, the well is still in the acceptable range, and it is allowed to activate the conventional well risk evaluation mode.

Leakage may take place in different spaces (See Figure 24).In some cases, leakage is likely to occur in a space which passes through a safety valve (See Figure 25).

**Figure 23. Schematic diagram of leakage from different spaces.**

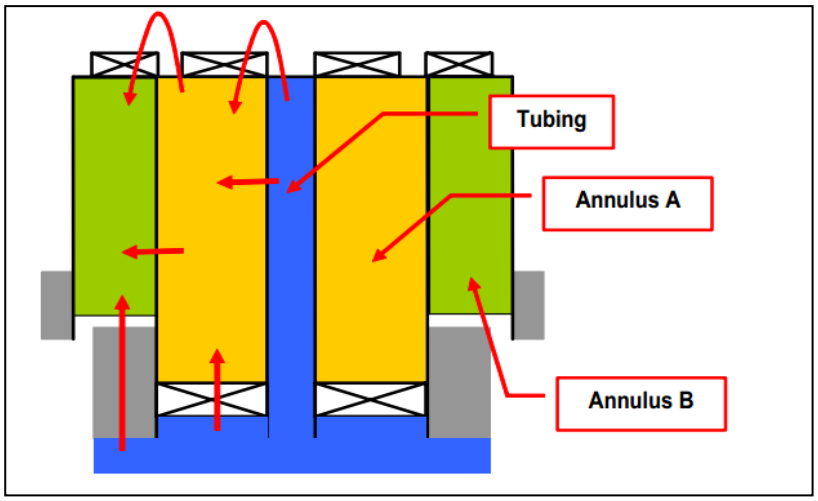


**Figure 24.Schematic diagram of leakage from one space.**

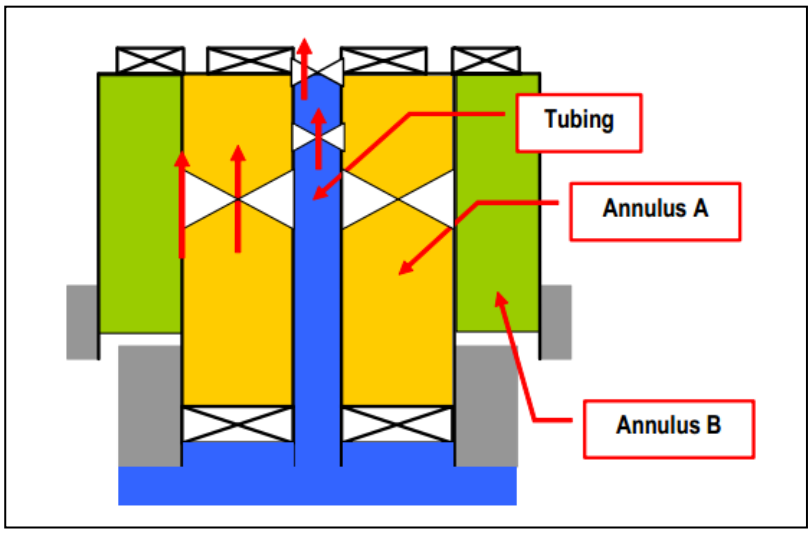

## 4.3 Well integrity evaluation mode

### 4.3.1 Construction of hierarchical structure

The Analytic Hierarchy Process (AHP) was developed by Thomas L Saaty, an American operations researcher, in the 1970s. Its premise is to deconstruct the elements related to decision-making across different layers (targets, criteria, schemes, etc). Based on this concept, a decision can be made by quantitative and qualitative analysis. The evaluation factors in the evaluation unit, which may affect the well integrity, are further divided into 13 influential factors. The hierarchical structure of well integrity risk evaluation is established, as shown in Figure 25. In this structure, the top layer is the target layer, namely integrity risk; the middle layer is the criterion layer, namely evaluation units of well integrity; the bottom layer is the scheme layer, namely influential factors.

**Figure 25. Hierarchical structure of integrity risk evaluations**

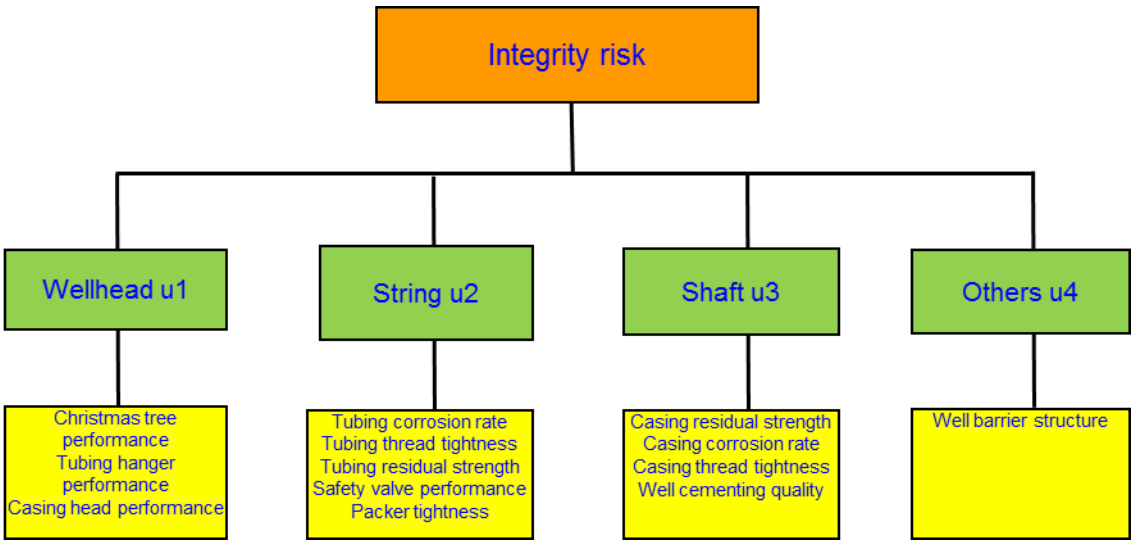


### 4.3.2 Construction of judgment matrix

From the hierarchical structure, we can determine the hierarchical model, deduce the relationship between different layers, and get the weight of each evaluation unit and factor.

By comparing the importance of evaluation unit u1, u2, u3 and u4 relative to integrity risk and assigning the value from scale values 1 to 7, we can derive scale values and their meanings (See Table 4) and obtain the matrix A for judging the importance of the index of criterion layer.

**Table 3. Meaning of each scale of hierarchical structure of integrity evaluation.**

| Level of Importance | Scale Value |
|---|---|
| Compared with j, the element i, is equally important. | 1 |
| Compared with j, the element i, is more important. | 3 |
| Compared with j, the element i, is far more important. | 5 |
| Compared with j, the element i, is extremely important. | 7 |
| If the ratio of the importance of element i to that of j is aij, then the ratio of the importance of element j to that of i is aji, where aji=1/aij | 1/3,1/5,1/7 |
| Expresses the median of adjacent judgments | 2,4,6 |

$$A=\left(a_{ij}\right)_{4\times4}=\begin{pmatrix}1 & a_{12} & a_{13} & a_{14}\\ 1/a_{12} & 1 & a_{23} & a_{24}\\ 1/a_{13} & 1/a_{23} & 1 & a_{34}\\ 1/a_{14} & 1/a_{24} & 1/a_{34} & 1\end{pmatrix}=\begin{pmatrix}1 & 3 & 5 & 7\\ 1/3 & 1 & 3 & 5\\ 1/5 & 1/3 & 1 & 3\\ 1/7 & 1/5 & 1/3 & 1\end{pmatrix} \quad (4)$$

## 4.4 Weight calculation

The value of each eigenvector of judgment matrix A is the weight of evaluation unit u1, u2, u3 and u4 relative to the target layer. The validity of the evaluation layer must be judged by consistency check and the judgment criterion is CR<0.1.

$$C_R=\frac{C_l}{R_l} \quad (5)$$

$$C_l=\frac{\lambda-n}{n-1} \quad (6)$$

Where:

Rl ——Proportional coefficient, relevant to matrix order n;

Cl——Consistency judgment criterion;

$\lambda$ ——Maximum characteristic root of judgment matrix.

The maximum characteristic root of judgment matrix A is expressed as $\lambda$ = 4.1170. By looking up the table, if Rl=0.90 for a 4-order matrix, then Cl=0.043<0.1. The characteristic vector with maximum characteristic root that meets the consistency requirement is expressed as Wmax= (0.88800.41210.18470.0869)$^{T1}$.

The normalised weight is expressed as Wmax = (0.47460.30860.16150.0553)T or the weight of string (u2), shaft (u3), wellhead (u1) and well barrier structure (u4) in gas well integrity is 47.46 per cent, 30.86 per cent, 16.15 per cent and 5.53 per cent respectively.

1 T= matrix transposition

### 4.4.1 Calculation of weight of influential factor

**Table 4. Integrity risk evaluation weight.**

| Item | | Element | Weight |
|---|---|---|---|
| 1 | Wellhead | Christmas tree performance | 9 |
| 2 | | Tubing hanger performance | 5 |
| 3 | | Casing head performance | 2 |
| 4 | String | Tubing corrosion rate | 12 |
| 5 | | Tubing thread tightness | 12 |
| 6 | | Tubing residual strength | 8 |
| 7 | | Safety valve performance | 8 |
| 8 | | Packer tightness | 7 |
| 9 | Shaft | Casing residual strength | 5 |
| 10 | | Casing corrosion rate | 2 |
| 11 | | Casing thread tightness | 10 |
| 12 | | Well cementing quality | 14 |
| 13 | Others | Well barrier structure | 6 |

The weight of each influential factor can be calculated by the aforementioned method. The normalised weight of wellhead-related factors (Christmas tree performance, tubing hanger performance and casing head performance) is expressed as: Wmax = (0.54620.33840.1154)T. The normalised weight of string-related factors (tubing corrosion rate, tubing thread tightness, tubing residual strength, safety valve performance and packer tightness) is expressed as: Wmax = (0.25810.25810.16450.1750.1443)T. The normalised weight of shaft-related factors (casing residual strength, casing corrosion rate, casing thread tightness and well cementing quality) is expressed as: Wmax = (0.17530.06030.31940.4630)T.

The weight of evaluation unit is multiplied by the weight of each influential factor to get the final weight of each influential factor. See Tables 7 and 8.

**Table 5.Integrity Risk Evaluation Summary.**

| Type | Evaluation Indicator | Performance Requirement | Monitoring Method | Reference Standard |
|---|---|---|---|---|
| Well head unit | Christmas tree performance | Good function and sealing performance | Valve leakage test and annular pressure monitoring | APIRP14B |
| | Tubing hanger performance | Good sealing performance | Annulus monitoring | APIRP90 |
| | Casing head performance | Good sealing performance | Annulus monitoring | APIRP90 |
| String | Tubing corrosion rate | Corrosion resistant | Corrosion coupon method | APIRP90 |
| | Tubing thread tightness | Good sealing performance | Air-tightness test technique | APIRP90 |
| | Tubing residual strength | Strength | Acoustic imaging logging | APIRP90 |
| | Safety valve performance | Good function and sealing performance | Valve leakage test and annular pressure monitoring | APIRP14B |
| | Packer tightness | Good sealing performance | Annulus monitoring | APIRP90 |
| Shaft | Casing residual strength | Strength | Acoustic imaging logging | APIRP90 |
| | Casing corrosion rate | Corrosion resistant | Corrosion coupon method | APIRP90 |
| | Casing thread tightness | Good sealing performance | Air-tightness test technique | APIRP90 |
| | Well cementing quality | Good sealing performance | Acoustic amplitude logging | APIRP90 |
| Others | Well barrier structure | Integral well barrier | Annulus monitoring | APIRP90 |

### 4.4.2 Integrity risk evaluation classification

Furthermore, each influential factor was graded and its value range was determined. The conventional gas well risks are divided into 3 categories (See Table 9).

**Figure 26. Integrity Risk Evaluation Classification Process.**

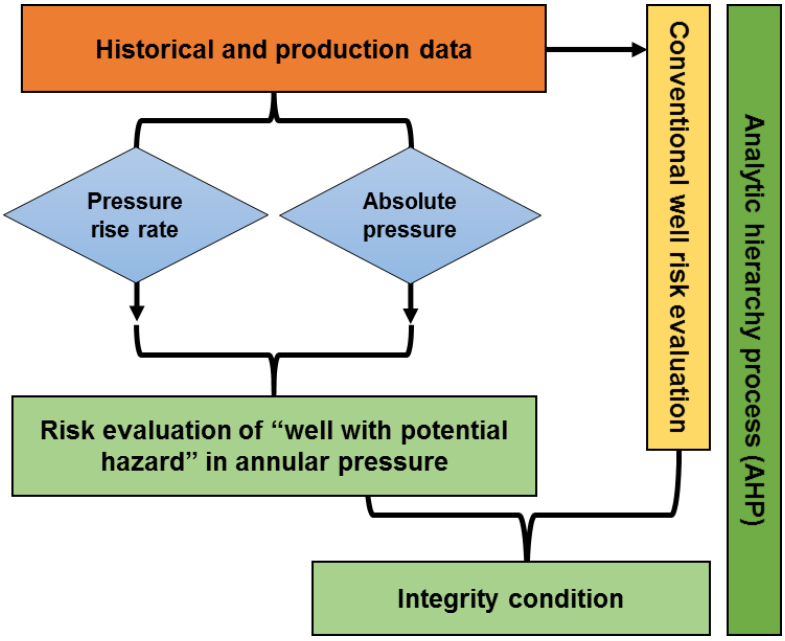


Based on research, the well integrity evaluation mode was established. As shown, the first step of integrity evaluation is initial classification of the well with reference to historic data and production data. This comprises risk evaluation of the "well with potential hazard" in annular pressure and the conventional well risk evaluation mode. This process will provide the evaluation result, and the solution (See Figure 26).

**Table 6.Integrity risk evaluation classification.**

| Risk Classification | Risk Weight Range | Integrity Condition |
|---|---|---|
| Ⅰ | >70 | Good |
| Ⅱ | 33~70 | Moderate |
| Ⅲ | ≤33 | Poor |

# 5 Jingbian County: Near-surface and surface monitoring

The main research objectives of the near surface and surface monitoring are:

- To clarify the response relationship between $CO_2$ concentration and soil or water quality, and discuss the relationship between the impact threshold and quantitative relation of near-surface environment factors of $CO_2$ leakage
- To develop the evaluation index system and method of near-surface environmental impact of $CO_2$ leakage through near-surface environmental monitoring and laboratory simulation study
- To establish a surface base method for $CO_2$ leakage detection.

## 5.1 Environmental baseline assessment

### 5.1.1 Land use investigation

The research area is located in the mountainous hilly-gully region in the southeast of Jingbian. It covers an area of 17,757.91ha, including the sequestration operation area (1,343.8h). The sequestration area accounts for 7.57 per cent of the total research area.

The $CO_2$ injection area is dominated by agricultural land (1,295.25ha), followed by construction land (34.82ha, primarily urban & rural construction and mining) and natural reserves (13.74ha). The three types of land respectively account for 96.39 per cent, 2.59 per cent and 1.02 per cent of the area of the gas injection area.

**Vegetation investigation**

In August 2012, the investigation team conducted a three day field investigation on the vegetation distribution in the whole research area, especially in the $CO_2$-EOR injection area. In the process of investigation, it randomly selected 10 typical quadrat points as the representative vegetation types in this area, and recorded the parameters of each quadrat point (area/longitude/latitude/altitude/slope of each quadrat point, plant species/quantity/coverage in statistical quadrat, etc).

The main basis for drawing the vegetation map of the experimental area was the existing vegetation classification system. Available 1:25,000 remote sensing imagery was interpreted. Based on the location of the experimental area and its surroundings and the field fixed-point quadrat investigation, referring to the vegetation distribution pattern, the interpretation keys of different vegetation types in the evaluation area were established for vegetation interpretation and vegetation map plotting.

Main herbaceous species around quadrat investigation areas including *Heteropappus altaicus* (Willd) *Novopokr, Setaria viridis* (l.) *Beauv*., *Melilotus officinalis* (Linn.) *Pall*., Shrubs and half shrubs including *Caragana korshinskii* Kom, *Salix psammophila* Wang et Yang, *Atemisia arenaria* DC. etc; Trees are *Populu Simonii* Carr., *Salix matsudana*, *Ulmus pumila l*., *Malus pumila* Mill., *Zizyphus jujuba*, etc.

### 5.1.2 Soil investigation

**Sampling method**

1. Sequestration area

Sampling points were distributed in four geomorphological positions (including the top of mountain ridge, the slope of mountain ridge, gully slope, and gully valley) depending on the difference of geomorphological position. Sampling points were distributed in the forest and grassland and the farmland depending on the

difference in land use. As there is no farmland in the gully slope, a total of seven sampling points were distributed in the gas injection area. See Table 8 and Figure 27.

**Table 7.Distribution of soil sampling points in sequestration area.**

| | Geomorphological Position | Land Use Type | Remarks |
|---|---|---|---|
| **1** | Top of mountain ridge | Forest and grassland | Top gentle slope |
| **2** | | Farmland | |
| **3** | Slope of mountain ridge | Farmland | Gentle slope |
| **4** | | Forest and grassland | |
| **5** | Gully slope | Forest and grassland | Steep slope |
| **6** | Valley bottom | Forest and grassland | Warping dam |
| **7** | | Farmland | |

**Figure 27. Sampling points in Jingbian sequestration area (Source: Google Earth).**


2. Greater research area

Sampling points were distributed in geomorphological positions (eg, river bottom, terrace, gully slope and top of mountain ridge) from the lowest point to the highest point of this area, depending on two land use types (farmland and forest/ grassland). As there is neither forest nor grassland in the lowest gully valley nor farmland in the gully slope, six sampling points were distributed in the research area. See Table 9 and Figure 28.

**Table 8. Distribution of soil sampling points in research area.**

| | Geomorphological Position | Land Use Type | Remarks |
|---|---|---|---|
| **8** | Valley bottom | Forest and grassland | Warping dam-11 |
| **9** | Slope of mountain ridge | Farmland-10 | Terrace |
| **10** | | Forest and grassland-9 | |
| **11** | Gully slope | Forest and grassland | Steep slope-8 |
| **12** | Top of mountain ridge | Farmland | Top gentle slope |
| **13** | | Forest and grassland | |

**Figure 28. Sampling points in research area. Yellow pin is the oil production site. (Source: Google Earth).**


## Content analysis of common ions in soil

**Table 9. Content of Major Ions in Topsoil and Subsoil in Research Area Unit: mEq/kg.**

| | $K^+$ | $Na^+$ | $Ca^{2+}$ | $Mg^{2+}$ | $CO_3^{2-}$ | $HCO_3^-$ | $SO_4^{2-}$ | $Cl^-$ |
|---|---|---|---|---|---|---|---|---|
| **Topsoil** | 0.264 | 0.343 | 4.958 | 0.7 | 0.09 | 4.829 | 0.425 | 1.073 |
| **Subsoil** | 0.195 | 0.437 | 4.408 | 0.833 | 0.145 | 4.699 | 0.406 | 1.093 |
| **Average** | 0.229 | 0.39 | 4.683 | 0.767 | 0.118 | 4.764 | 0.416 | 1.083 |
| **Relative difference/%** | 26.21 | 21.39 | 11.09 | 16 | 37.93 | 2.68 | 4.41 | 1.8 |

Table 10 shows major ions in the topsoil and subsoil in the research area and their average content. From this table, we can know that major anion in the soil of the research area is HCO3- (4.863mEq/kg), followed by Cl-, CO32- and SO42- with lower content; the major cation is Ca2+(4.764mEq/kg), followed byMg2+, K+ and Na+ with lower content. Topsoil has higher content of K+, Ca2+, HCO3- and SO42- than subsoil. Subsoil has higher content of Na+, Mg2+, CO32- and Cl- than topsoil. The largest difference (37.93 per cent)

between topsoil and subsoil lies in CO32-, followed by K+, Na+ and Mg2+, all of which are low-content minor ions. There is a small difference in two major ions Ca2+ (10.09 per cent) and HCO3- (2.68 per cent). To sum up, the difference in major soil ions is small in the research area.

### 5.1.3 Water environment investigation

**1. River water quality investigation**

A river flows through the Shazui Dam at Point 7 of the research area (Figure 27). The river dries out in spring, so summer monitoring data was used for analysis, when the dam is likely to hold water.

I. Acidity/ alkalinity and hydrochemical type

The pH value of the water sample at Point 7 measured in spring is 8.53, indicating slight alkalinity. This value reaches the criteria of Class III water specified in the Environmental Quality Standards for Surface Water (GB3838-2002). From the monitored values of major ions in the water sample collected from Point 7, we can assume that the hydrochemical type is chloride- sulfuric acid-sodium bicarbonate water.

II. Organic pollutant

According to Class III standard of the Environmental Quality Standards for Surface Water (GB3838-2002), the COD (Chemical Oxygen Demand), BOD (Biochemical Oxygen Demand) and permanganate index of water sample 7 was evaluated by the single factor index method. The single factor index of COD, BOD and permanganate index is 0.45, 1.4 and 0.0415 respectively. BOD5 is out of specification.

III. Heavy metal analysis

According to the Class III criteria specified in the Environmental Quality Standards for Surface Water (GB3838-2002), 7 heavy metals (Mn, Cu, Zn, As, Cd, Ni, Pb and Hg) of water sample 7 were evaluated. The single factor index of Mn, Cu, Zn, As, Cd, Ni, Pb and Hg is 0.192, 0.108, 0.364, 0.028, 0.0176, 0.0418 and 0.73 respectively. Heavy metal content is within the bounds of water quality standards.

IV. Analysis of nutrient elements

The single factor indexes of three plant nutrients (Total nitrogen (TN), total phosphorus (TP) and nitrate) of water sample seven are 5.572, 0.06 and 0.489 respectively. TN is outside typical quality standards.

**2. Drinking water quality investigation**

I. Acidity/ alkalinity

The pH value of the water sample 1 collected from Xuejiapan (Figure 27) is 8.02 in spring and 7.99 in summer. The pH value of the water sample 2collected is 7.99 in spring and 8.28 in summer, ranging between 6 and 9. All values reach the Class III criteria specified in the Quality Standard for Ground Water (GB/T14848-93).

II. Total hardness

Total hardness is an important reference for judgment of water quality. It often describes the content of calcium ion (Ca2+) and magnesium ion (Mg2+). In normal cases, total hardness is the sum of carbonate hardness and non-carbonate hardness. According to the hardness (in terms of CaCO3) rating criteria, groundwater is divided into soft water (<150mg/L), slightly hard water (150 - 300mg/L), hard water (300 - 450mg/L) and very hard water (>450mg/L). Table 11 shows the total hardness test results of 2 underground drinking water samples collected from the research area in spring and summer.

**Table 10. Total Hardness test results of underground drinking water samples in spring and summer (mg/L).**

| Water Sample No. | Sampling Location | Spring | Summer | Groundwater Quality Criterion Class III Limit |
|---|---|---|---|---|
| **1** | Peasant household from Xuejiapan | 33.5 | 165.4 | ≤450 |
| **2** | Oil production crew | 20.1 | 105.4 | |

From Table 11, the hardness at these two sampling points in summer is higher than that in spring. The drinking water sample 1 collected from Xuejiapan is soft water in spring and slightly hard water in summer. The water sample 2 collected by the oil production crew is all soft water. The total hardness of drinking water in spring and summer is lower than the limit value of Class III water specified in the Quality Standard for Ground Water (GB/T14848-93). The hardness change of underground drinking water is related to groundwater recharge, geological and hydrological conditions.

III. Heavy metal

**Table 11. Heavy Metal test results of underground drinking water samples in spring and summer (ug/L).**

| Heavy Metal | Farmer's household from Xuejiapan | | Oil production crew | | Class III Limit (mg/L) |
|---|---|---|---|---|---|
| | Spring | Summer | Spring | Summer | |
| **Mn** | 1.92 | 0.7 | 16.5 | 1.64 | ≤0.1 |
| **Cu** | 10.3 | 3.82 | 2.54 | 8.81 | ≤1.0 |
| **Zn** | 33.2 | 3.23 | 27.4 | 16.2 | ≤1.0 |
| **Cd** | 0.20 | ＜0.01 | 0.14 | ＜0.01 | ≤0.01 |
| **Pb** | 13.7 | ＜0.01 | 3.00 | 2.14 | ≤0.05 |
| **As** | 2.25 | 2.13 | 2.16 | 1.87 | ≤0.05 |
| **Hg** | 0.034 | 0.424 | 0.054 | 0.077 | ≤0.001 |

The heavy metal monitoring results of underground water samples collected from two sampling points in the research area are listed in Table 12. As heavy metals in surface water, heavy metals in underground drinking water in the research area were also evaluated by the single factor index method in accordance with Class III criteria specified in the Quality Standard for Ground Water (GB/T14848-93). The results of evaluation on pollution from seven heavy metals (Mn, Cu, Zn, Cd, Pb, As and Hg) in underground drinking water samples are listed in Table 12.

**Table 12. Calculation results of heavy metal pollution index of surface water samples in spring and summer.**

| Heavy metal | Farmer's household from Xuejiapan | | Team 3 of oil production crew 4 | |
|---|---|---|---|---|
| | Spring | Summer | Spring | Summer |
| **Mn** | 0.0192 | 0.007 | 0.165 | 0.0164 |
| **Cu** | 0.0103 | 0.0038 | 0.0025 | 0.0089 |

| | | | | |
|---|---|---|---|---|
| **Zn** | 0.0332 | 0.0032 | 0.0274 | 0.0162 |
| **Cd** | 0.02 | 0.001 | 0.014 | 0.001 |
| **Pb** | 0.274 | 0.0002 | 0.06 | 0.0428 |
| **As** | 0.045 | 0.0426 | 0.0432 | 0.0374 |
| **Hg** | 0.034 | 0.424 | 0.054 | 0.077 |

From Table 12, the results show that all the heavy metal content in the two underground drinking water monitoring samples collected in both spring and summer are within quality standards and all values reach the Class III criteria specified in the Quality Standard for Ground Water (GB/T14848-93).

## 5.2 $CO_2$ leakage detection method

There are two $CO_2$ leakage scenarios: sudden extensive leakage and long-term slow leakage. During $CO_2$ injection, which involves drilling and equipment installation process, possible $CO_2$ leakage could include equipment leakage, injection pipe leakage and injection shaft leakage. Each of these is sudden extensive $CO_2$ leakage. The $CO_2$ gas could accumulate to high enough concentrations to be toxic with obvious physiological toxicity to humans and wildlife. As the density of $CO_2$ is 1.52 times denser than air, the volume of $CO_2$ that leaks may be estimated with the heavy gas model or toxic and harmful gas models.

Following the assessment of potential leakage at the research site, two near-surface $CO_2$ concentration detection methods and one near-surface $CO_2$ concentration monitoring methods were selected.

The $CO_2$ capture equipment and method for $CO_2$ leakage detection designed for this project was deemed suitable for continuous and massive capture of air-borne $CO_2$ in the open air. The $CO_2$ capture devices include:

- NaOH solution stored in liquid bottles and including a collection bag and perfusion tube that connects bottles and bags
- air flows into a NaOH solution bottle
- velocity of the NaOH solution controlled by a regulating valve, with insolubles removed by a filter
- monitoring the flow velocity of the NaOH solution by dropper, and inhibition of gas into the collection bag by vent.

After sampling, an isotope mass spectrum analyser for testing 13C and 14C values was used. This sampling method can improve the 13C and 14C determination sensitivity. This method also works to eliminate the interference from near-surface and air-borne oil components (hydrocarbon compound). This sample collection method in combination with the curve tracing method (Michelucci and Faudot, 2005) is an effective approach to judge the source of $CO_2$, so it is worthy to be widely applied. The sequestration injection area was inspected by this method and no leakage was found.

For remote regions, an autonomous soil gas sampler with automatic remote data transmission was built and used for analysis. This $CO_2$ analysis system established for this project has the protection grade above IP31 (Reference standard GB 4208-2008/IEC 60529, testing instrument protection grade) and is waterproof and applicable for use in wet soil. The sampler can measure ranges from:

- carbon balance pressure 0.1 to 100 kpa;
- carbon dioxide concentration 4.4 PPM to 1760 PPM.
- Output signals: 0 to 5 v.
- Power supply: 6 V, about 3 w power consumption, the indicators system meet the design requirements.

It allows long-distance transmission and unattended continuous automatic monitoring. It is important to note that the system software can be connected to 32 monitoring points simultaneously. The data measured from these 32 monitoring points can be used for discovery and judgment of $CO_2$ leakage points.

The online water-borne $CO_2$ monitoring system is also waterproof and applicable to use in wet soil. Similarly, it is not necessarily attended and it allows long-distance transmission and unattended continuous automatic monitoring. This system is applicable for long-term unattended groundwater monitoring around the $CO_2$ sequestration wellhead. It provides a tool to judge the impact of $CO_2$ leakage on water quality.

Despite the monitoring technologies currently used, the probability of sequestrated $CO_2$ leakage is low. The most probable leakage is long-term slow $CO_2$ gas leakage. In this case, $CO_2$ gas may not accumulate to produce obvious physiological toxicity. So it is obviously inappropriate to use the heavy gas diffusion model or the toxic and harmful gas diffusion model because rates of leakage too low for modelling. The only approach is to dispose a small quantity of $CO_2$ gas leakage as atmospheric pollutant and estimate the leakage volume with the Gaussian Inverse Model for future accounting purposes.

## 5.3 Seismic monitoring technology

4D seismic monitoring technology is a preferential choice for observing, monitoring and validating the safety of sequestration. In this technology, a seismic acquisition survey is conducted before injecting $CO_2$ into the oilfield, then intermittently when reaching certain injection volumes or a certain time of injection, and finally after sequestration. After that, the seismic data of different periods in time and amplitude are compared. From the differences found between the data, the $CO_2$ distribution range, pressure, sequestration capacity and oil displacement efficiency are determined. Yanchang Petroleum did not complete background seismic acquisition in Qiaojiawa Block of Jingbian Oilfield. In contrast, the background measurement data obtained by seismic monitoring in Yougou Block of Wuqi Oilfield was acquired in June 2015 and is now being interpreted. For this report only the Yougou Block seismic acquisition program will be discussed.

### 5.3.1 Technical difficulty of loess tableland seismic acquisition

The Yougou Block located in the mid-south of the North Shaanxi Slope of the Ordos Basin is classified as loess tableland. Loess (aeolian sediment formed by the accumulation of wind-blown silt) tableland is one of the key and difficult areas of oil and gas exploration in this region. The super-thick loess tableland of North Shaanxi is as thick as 400m, and the loess is loose and dry. The loess tableland seismic exploration is a well-known world-class problem. In decades, no progress has been made in seismic exploration of this area. The difficulty of seismic acquisition is mainly because of severe surface absorption and attenuation, multi-wave interference, meaning it is hard to get a good seismic response. As a result, oil and gas exploration in this region has been restricted to drilling exploration and geological interpretation.

Traditionally to overcome poor seismic response, seismic acquisition has been crooked and curved following the valleys and channels, where the seismic signal is better. But a closed loop, required for 4D seismic acquisition typically cannot be completed, which makes the data interpretation difficult. The low quality data makes reservoir inversion processing of the seismic data also challenging. However, after years of exploration, some progress has been made in seismic acquisition, processing and interpretation in the Ordos Basin. In the acquisition stage, appropriate excitation points and conditions were selected and the observation system was arranged properly. In the processing stage, fine correction of first arrival refraction wave statics was made. In the interpretation stage, the target evaluation was conducted by variable velocity mapping and reservoir prediction. Available seismic data have clear profile layers, definitive breakpoints and high signal-to-noise ratio (SNR), which is a substantial breakthrough.

### 5.3.2 Geological base of loess tableland seismic exploration

Aeolian loess can be classified into primary loess and secondary loess. The accumulation of primary loess which has been modified since Holocene is called secondary loess.

1. Main geological features of loess: Light greyish yellow or brownish yellow, mostly composed of silty sand, uniform texture, loose and porous structure, visible porosity; unstratified; calcium-rich, vertical joints developed, loose physical structure.
2. Geomorphic features: Complicated geomorphologic landscapes as a result of the combination of various kinds of gullies, ridges, tablelands, loess hills, slopes and rivers. In the main, they take the shape of tree branches and other fauna.
3. Physical properties: Dry loess velocity: 300~650m/s; wet loess velocity: 800~1,000m/s; aqueous loess velocity: 1,300~1,800m/s; Paleogene - Neogene laterite: 1,600~2,200m/s; Mesozoic rocks: 3,000~3,500m/s. (Gonghe Lv,2001) gave the physical parameters of the near-surface and shallow strata in test area (Table 13)

**Table 13. Physical properties of near-surface and shallow strata in loess tableland (Gonghe Lv, 2001).**

| Horizon | Stratigraphic Thickness (m) | Velocity (m·s-1) | Density (g·m-3) | Absorption Coefficient |
|---|---|---|---|---|
| **Low-velocity layer or weathered layer (secondary loess)** | 13~16 | 310~400 | 1.3~1.39 | 15 |
| **Sub-weathered layer (secondary loess)** | 100~400 | 710~1,100 | 1.6~1.79 | NA |
| **High-velocity layer (rock stratum)** | - | 3,150 | 2.3 | 171 |

### 5.3.3 Technical difficulty of loess tableland seismic exploration

**1. Technical difficulty of seismic acquisition**

I. Poor seismic excitation conditions: In the loess tableland, most of the seismic wave energy is absorbed in the sediment's void area and is due to the plastic deformation response of the sediment. Only a small amount of energy disperses due to elastic deformation, so the capability of effective waves is restricted and interference waves occur (eg, surface wave appear). Literally, seismic excitation conditions change fast.

II. Seismic wave absorption and attenuation: The super-thick loess is loose and dry and relatively low in differential compaction degree with a porosity of 30 per cent to 50 per cent with pores filled with air a great deal of gas and moisture. The effect of intergrain liquid/gas extrusion and burst could lead to a strong impact of energy consumption on seismic wave absorption and attenuation. According to the empirical formula, the correlation between stratigraphic absorption factor and longitudinal wave is:

$Q \approx 14vp2.2$ (equation number not given as per other sections)

III. Where: Q - stratigraphic absorption factor; vp - longitudinal wave, km/s. The absorbability quality factor of the loess stratum and the lower Mesozoic stratum is about 15 and 171 respectively, meaning that the seismic wave in the loess stratum has the highest absorption and attenuation rate. The absorption and attenuation of 15m-thick loess stratum is equivalent to that of the 1500m-thick deep old stratum. So, the main attenuation of Loess area is mainly attenuation of the loess layer.

IV. Near-surface strong interference wave: Loess has a loose structure, low velocity, large porosity and deep water table. This leads to severe anisotropy of medium and easily causes the generation of strong interference. One is regular interference, such as surface wave, refracted wave, multiple-refracted reflection wave. Next is secondary interference, such as scattering interference arising from air effect in loess pore space and severe secondary interference arising from dramatic undulation of the surface terrain.

V. Difficult conditions for seismic construction: Due to complicated terrain and crisscrossed ravines and gullies, it is difficult for construction machinery to enter the site. The fixed trace spacing of conventional seismic cables is hard to adapt to the frequent change of the terrain. Poor visibility results in many blind spots and high GPS survey exploration cost, and low operation efficiencies.

**2. Technical difficulty of loess tableland seismic processing**

The existence of technical difficulty of loess tableland seismic acquisition leads to too low SNR of seismic data of this type of region, serious problem with static correction, etc.

I. Static correction

The terrain of loess tableland changes sharply, the lateral changes of excitation and receiving conditions occur quickly, the thickness and velocity of the near-surface weathered/sub-weathered layer is unstable, the top interface of the high-velocity layer is unstable, and the static correction problem is outstanding. Conventional static correction methodology cannot adapt to the loess tableland, because it is difficult to obtain sufficient information about the speed and thickness of the underground weathered/sub-weathered layer; and, it is also difficult to fully meet such a requirement of Greenmount which is one software for refraction static correction that there shall be a stable refraction interface.

II. Too low data SNR

Loess medium is far from an ideal elastic medium. Due to the limitation of construction cost and period, the shothole excitation depth hardly goes below the water table. As the energy excited by the shothole is difficult to diffuse downwards, the overwhelming majority of it is transformed into the energy for loess caving, forming very strong surface wave, refracted wave, multiple-refracted reflection wave (also called loess resonance or ringing) and lateral wave echoing between valleys and secondary interference. The strong effect of seismic wave absorption and attenuation to the near-surface and shallow strata of loess tableland results in weak energy of deep effective reflection wave, etc. Due to these factors, the seismic data of loess tableland produces typically low SNR data, which is difficult to process.

III. Fast high-frequency absorption and attenuation

The lithology excited in the loess tableland is characterised by looseness and low velocity. It may take a long time for the vibration generated after explosive blasting to convert into elastic waves, so it is difficult to excite high-frequency signals and strong energy. Moreover, loess is loose. Where: Q - stratigraphic absorption factor; vp - longitudinal wave, km/s. The absorbability quality factor of the loess stratum and the lower Mesozoic stratum is about 15 and 171 respectively, meaning that the seismic wave in the loess stratum has the most serious absorption and attenuation. The absorption and attenuation of 15m-thick loess stratum is equivalent to that of the 1,500m-thick deep old stratum. So, the principal ground attenuation of the loess tableland is the attenuation of the loess stratum.

IV. Near-surface strong interference wave:

Loess has loose structure, low velocity, large porosity and a deep water table. This leads to severe anisotropy of the medium and easily causes the generation of strong interference. One is regular interference, such as surface wave, refracted wave, multiple-refracted reflection wave. Another is secondary interference, such as scattering interference arising from the air effect in loess pore and severe secondary interference arising from dramatic undulation.

## 5.4 Seismic acquisition scheme of Yougou Block of Wuqi Oilfield

### 5.4.1 Geological requirements

1. The major target stratum for seismic acquisition is the Chang-4+5 reservoir (Table 14) of which the depth is approximately 1940-2040m, supplemented with Chang-3to Chang-7 reservoirs (1,750-2,300m). This reflects the real structural characteristics, sand body distribution characteristics and natural fracture development characteristics and meets the need of geological research of $CO_2$ displacement.
2. This meets the need to forecast the gas-bearing property of Chang-4+5 reservoir in Yanchang Formation of Wu-38 Well Area of Wuqi Oilfield.
3. By processing and interpreting 3D seismic acquisition data, conduct the seismic background data study before injecting the $CO_2$ gas for 3D seismic monitoring.

**Table 14. Technical indexes of major target stratum.**

| Major Target Stratum | Buried Depth (m) | Distinguishable Fault Throw (m) | Distinguishable Thickness (m) | Basic Frequency (Hz) | Bandwidth Range (Hz) |
|---|---|---|---|---|---|
| Chang-4+5 reservoir in Triassic Yanchang Formation | 1940-2040 | 50 | 15 | 36 | 10-80 |

### 5.4.2 Overview of work area

In 2014, Yanchang Petroleum deployed 3D seismic acquisition (See Figure 29/30) in an area of 10.68km² (full fold) of Lower Yougou, Zhangguanmiao Township in the southwest of Wuqi County (See Figure 29).

The work area reconnaissance shows that this area is a part of the ridge-like hill and gully region of loess plateau, with altitude of 1,400-1,700m and relative height difference of 150-200m. The width of loess tableland is generally 50-100m; the top elevation of tableland is 1,500-1,700m, only 20-30m in the seriously-eroded section. The ridge is narrow and the slope is steep. For these factors, the geomorphologic landscapes of massive mountains and deep valleys, fragmented landform and crisscrossed ravines and gullies have come into being (See Figure 30).

**Figure 29. Administrative Division Map of Work Area. (Source: Map published by the map of China publishing group)**

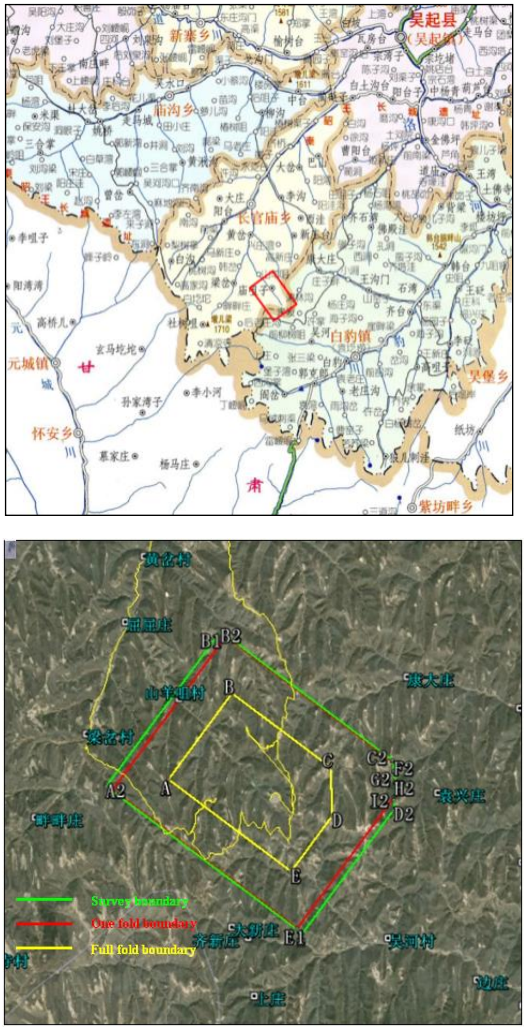


**Figure 30. Schematic Diagram of 3D Seismic Acquisition Range of Work Area (Source: Google Earth).**

**Figure 31. Traffic Roads in Work Area. (Source: Shaanxi Yanchang Petroleum).**

This area consists of two parts. The upper part, 5-20m, is Quaternary upper-Pleistocene loess, whilst the lower part is Quaternary middle-Pleistocene loess. Due to thick accumulation of loess, the pre-Quaternary stratum is somewhat exposed under the incised valley and steep slope (See Figures 31, 32 and 33).

**Figure 32.Crops and Vegetation. (Source: Shaanxi Yanchang Petroleum).**

**Figure 33. Surface Facilities in Work Area. (Source: Shaanxi Yanchang Petroleum).**

### 5.4.3 Technical difficulty

1. The strong effect of absorption and attenuation of the super-thick loess stratum makes it difficult for the seismic wave energy to propagate downward. This area has complicated landform. In this area, no ravine system is developed. The thickness of the loess stratum varies from tens of meters to hundreds of meters. The loess stratum is dry and loose and has low velocity. It has strong effect of seismic wave absorption and attenuation on seismic wave. This is unfavourable for excitation and receipt of seismic wave. From Figure 34, we can see that the single-shot energy is strong in the ravine and weak in the half-slope.

**Figure 34. Excitation energy distribution and terrain overlay of Loess tableland.**

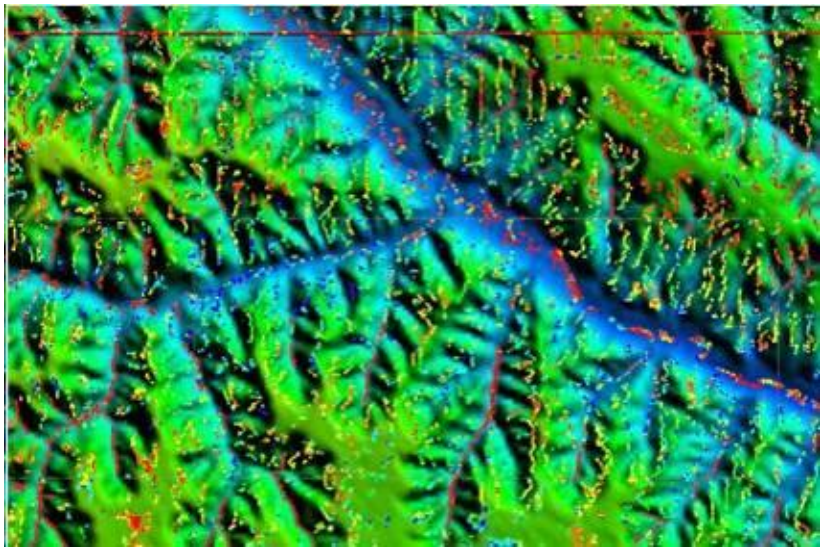

2. The excitation energy of slope area is weak, especially in the downdip direction

   The previous seismic data analysis reveals that the seismic data obtained by excitation of the slope area in the loess tableland has the worst effect. In the single-shot record, the half-SNR received in the downdip direction is lowest. The reason lies in that the predominant lithology of the slope area is secondary accumulation characterised by loose soil, with serious energy dissipation and poor excitation conditions. Due to the effect of inclined slope aspect, the large part of the projection faces the updip direction after explosive blasting, whether the energy directly transmitted towards subsurface or the energy reflected to the stratum when meeting the surface. This means most of the energy is received in the updip direction after subsurface reflection, and little energy is received in the downdip direction. This phenomenon becomes more serious as the general dip of the slope increases.

   As the elevation of the slope area decreases, the excitation point comes closer to the uppermost horizon of high-velocity layer and the loess becomes thinner, the absorptivity of loess presents the trend of linear decrease, while the energy projection window area presents the trend of exponential decrease. This causes the decrease of actual under-passing energy (See Figure 35).

**Figure 35. 3D excitation energy distribution sketch of a Loess tableland.**

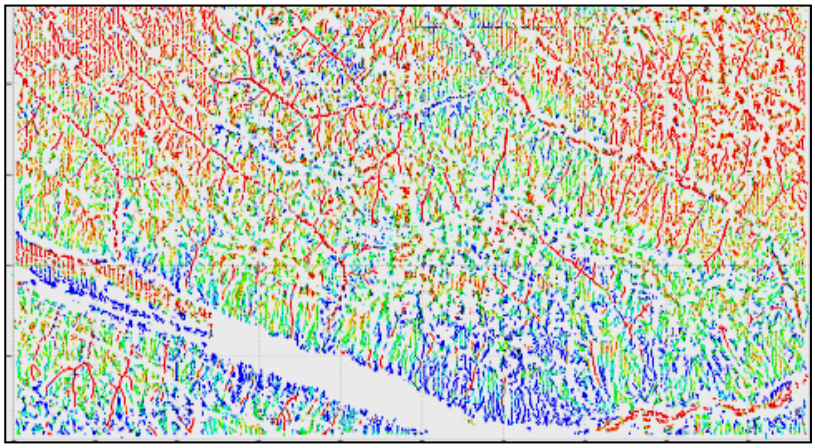

3. Complicated wavefield

   Due to the long-term scouring and cutting of rainwater, the surface loess causes the formation of discontinuous terrain points. As the variation of inter-layer compaction leads to anisotropy, the seismic wave field is complicated. For example, the shallow multiple refracted wave, secondary interference wave and random interference waves are strong.

4. Difficulty in static correction due to complicated surface structure and terrain

   The dramatic undulation of terrain, complicated and volatile surface structure, and super-thick weathered/sub-weathered layer and great lateral change leads to the extreme development of refracted wave, multiple reflected wave, surface wave and linear interference. This has an especially serious impact on the shallow layer, and makes it difficult to create an accurate geological model for the surface layer, as well as making it hard to conduct a static correction.

5. A large number of obstacles

   There is an abundance of oil drilling, production, gathering, transmission and supply facilities in the work area. The shot restriction area in the oil gathering station is longer than 400m in some cases.

6. How to avoid the impact on secondary acquisition, because secondary acquisition is necessary

   This project is a sequestration project. The second acquisition and excitation in the same position is required after some time. At that time, the data quality may be worse compared with that of the first time (See Figure 36).

**Figure 36. Single-shot effect after fragmentation of the lower part of excitation point.**

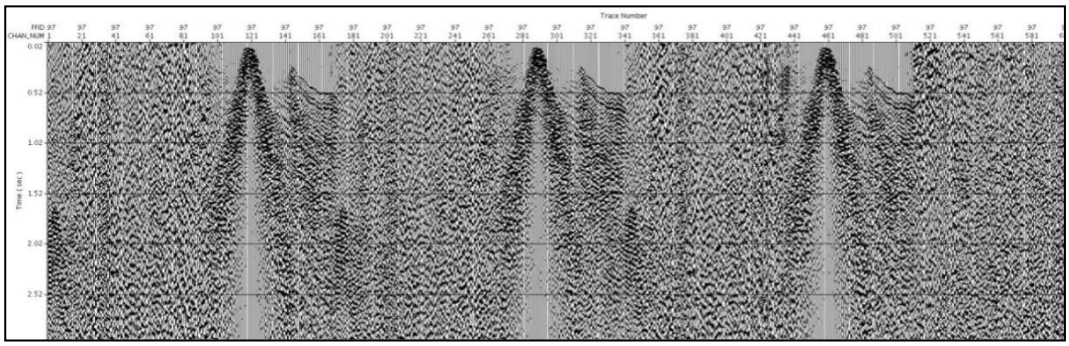

### 5.4.4 Technical strategy

**Strategy 1:** It is very important to find suitable surface lithology for excitation on the loess tableland. Better seismic data can be obtained by producing excitation beneath the clay layer or water table. The surface lithology investigation before production can provide the basis for designing the excitation well depth for each separated line.

The 32-Chinese-character excitation principle below shall be followed during field acquisition:

- Combined excitation - If a single well cannot meet the need, the solution is excitation through combination well.
- Avoid the high and select the low - Excite in the valley or depression when possible.
- Avoid the steep and select the gentle - Excite in the gentle area when possible.
- Avoid the dry and select the wet - Excite from the horizon with good water-bearing property when possible.
- Avoid yellow and select red - Excite from the area with red clay layer to ensure the excitation in this layer.
- Avoid the strong point and strike the weak point —— In case that the excitation in the aqueous loess and clay layer cannot be ensured, excite from primary loess when possible.

**Strategy 2**: In weakly elastic media like loess tableland, the seismic wave energy generated by explosive blasting has the most direct relationship with the surrounding-rock seismic wave propagation velocity. The excited seismic wave energy increases with the increase of the seismic wave propagation velocity of the lithology around the excitation point. For a flat tableland, the excitation is made in the red clay layer because the velocity in this layer is much higher than that in the upper and lower loess layer. The lithological structure for seismic acquisition is just the surface, and the velocity structure is the nature.

For construction of this work area, the fine investigation is made in the form of lithological investigation to draw the optimal excitation depth map. At the same elevation, preference is given to V-shaped gully bottom excitation. Excitation from a narrow ridge with the largest free plane or an isolated hill shall be avoided when possible. This is to ensure the energy produced by blast explosives is applied underground as more as possible.

**Strategy 3:** An appropriate geophone array base is selected for effective suppression of linear noise. During processing of seismic data, an appropriate noise suppression means is chosen to improve the SNR of seismic profile.

**Strategy 4:** Seismic wave attenuation investigation is made by the double deep-Uphole technique to provide an accurate basis for loess layer thickness calculation and tomographic inversion static correction. The Uphole method is a seismic survey method that uses receivers on the ground surface with an energy source buried deep in a well. The Uphole technique is typical for areas with low velocity layers, in the case the deep loess terrain.

**Strategy 5:** Before construction, the first is to use high-precision satellite pictures for indoor simulation of receiving line and shot point distribution, develop the across-obstacle geometry-variable design, analyse the target stratum fold, arrange and densify shot points in a reasonable manner, and ensure the target stratum can get enough reflection information. Where the shot restriction area with oversized obstacles is too large, the profile gap is minimised by the charge-reducing obstacle-approaching technique, for the sake of safety and quality. During construction, the survey and technical directors and the designer of each separated line conduct a detailed survey in advance to determine the scope of shot restriction, make a secondary geometry-variable design adjustment, and conduct the construction design without affecting the number of stacking folds in the absence of target stratum. Attention shall be paid to distribution of underground pipe network and avoidance of safety accidents.

**Strategy 6:** To ensure the consistency of acquisition data, the first data acquisition shall be use the parameters exactly the same as what are used in the second acquisition.

### 5.4.5 4D seismic requirements

Although seismic exploration has been implemented in this region for years, there is no mature technique to undertake seismic for sequestration. Application of geophysical techniques in gas migration monitoring is common in foreign countries, but is novel in this region. For 4D seismic, on the loess tableland the shot well array centre is maintained over the intervals of acquisition to ensure the consistency of the coordinates measured between times. However, to solve the problem existing with gully-bottom single-well excitation, the coordinates of the same pile measured two times (the actual values obtained after measured two times are smaller than half of surface-element side length) shall be provided.

Technical requirements on 4D seismic acquisition and processing ensure that

- the physical points for the present and next construction are consistent
- the coordinates are consistent (RTK measurement)
- the elevation is consistent (RTK measurement)
- well depth is consistent (measurement)
- the charge size and type of explosives are consistent
- the geophone pattern is consistent
- the physical point offset is consistent
- the equipment and parameters for the present and next construction are consistent
- the processing flow is consistent.

## 5.5 Baseline seismic acquisition of Yougou Block of Wuqi Oilfield

### 5.5.1 Operation of the work

**1. Surveying**

Major surveying work in the area began on March 3, 2015 and was completed on June 11, 2015 (lasting 103 days, including 79 days for actual production). More specifically, the instrument self-check was conducted on March 3, 2015; the control network was distributed in the period from March 4 to 6. It took 62 consecutive days from the start of formal survey line production on March 7, 2015 to the completion of formal survey line construction on May 17, 2015. The restoration of arrangement marks and verification of deviated shot point was conducted during the period from April 1 to June 11, 2015, (lasting 72 days).

**Figure 37. Location map of survey lines and shot points in 3d seismic acquisition project of Wu-38 Block, Wuqi County.**

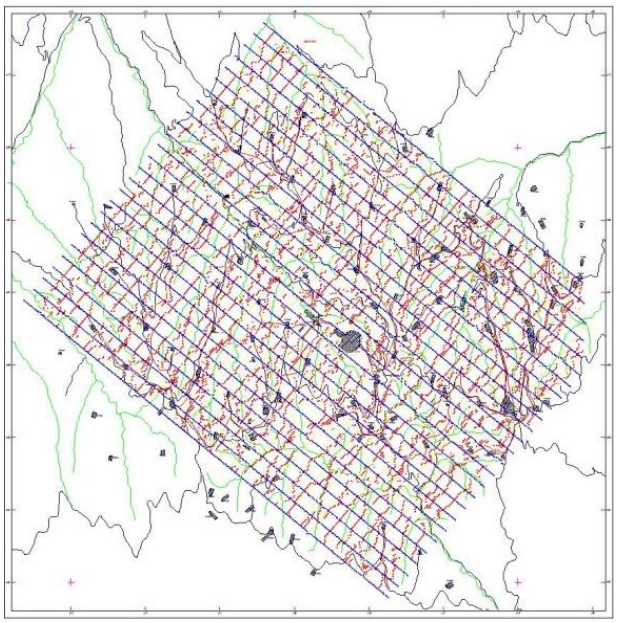

During work area survey, 25 swaths of 3D survey lines and 13,007 physical points were surveyed, with a total survey line length of 316.55Km (See Figure 37 and Table 15); 26 receiving lines and 6,567 receiving points were surveyed, with a total receiving line length of 163.525Km; 31 rows of excitation lines and 6,440 excitation points were surveyed, with a total excitation line length of 153.025Km.

A total of 466 points were resurveyed in the work area. The resurvey ratio was 3.58 per cent.

**Table 15.Statistical table of quantity of works.**

| Name | Quantity of Works | Name | Quantity of Works |
|---|---|---|---|
| Number of swath | 25 | Full fold area ($km^2$) | 10.68 |
| Number of receiving lines | 26 | Construction area ($km^2$) | 30.75 |
| Number of receiving points | 6,567 | Shot point area ($km^2$) | 28.71 |
| Number of shot lines | 200 | Number of Uphole points | 4 |
| Number of shot points | 6148 | Number of test points | 2 |

## 2. Surface investigation

Six Uphole points were completed in this work area. All (including 4 double-Uphole) were considered acceptable, corresponding to a 100 per cent acceptance rate. The first arrival of original seismic data is clear and the background is quiet. In data processing, the first arrival was picked by the human-computer interaction method and interpreted automatically by microcomputer, giving accurate and reliable results.

## 3. Seismic acquisition

In 2015, the Project Management Department of the 3D seismic exploration data acquisition project of Wu-38 Block in Zhangguanmiao, Wuqi deployed the full fold area of 10.68km2 and designed 6,148 excitation points and 6567 receiving points. 6177 physical points and two early-production test physical points (totally 47 shots) were completed for this project. Totally six Upholes were completed in the whole area (including four double-well Upholes).

### 5.5.2 Quality and technical indexes

For the 3D seismic data acquisition project, 3D full fold of 10.681km$^2$ was completed in this work area. 6,177 production records were obtained; all of them were acceptable, corresponding to the acceptance rate of 100 per cent. Two pre-production test physical points (including 47 shots) were completed. Six Upholes were completed, corresponding to the acceptance rate of 100 per cent. All quality indexes comply with the project technical design and specifications (See Table 16).

**Table 16. Statistics quantity of completed works.**

| Item | Design Quantity of Works | Quantity of Completed Works | Completion Ratio |
|---|---|---|---|
| **Number of full folds** | 144 | 144 | 100% |
| **Full fold area** | 10.681km$^2$ | 10.681km$^2$ | 100% |
| **Number of (pencils of) lines** | 25 | 25 | 100% |
| **Number of production physical points** | 6,148 | 6,177 | 100.47% |
| **Test physical points** | 47 | 47 | 100% |
| **Number of Uphole points** | 6 | 6 | 100% |

### 5.5.3 Time-effect analysis

Data acquisition in the work area began from 25 May 2015 and field acquisition was completed on 11 June 2015 - a process lasting 18 days with an average daily efficiency of 343 shots. The instrument field production took 18 days and daily instrument efficiency was 343 shots, with maximum daily production capacity of 1,039 shots (See Figure 38).

**Figure 38. Time-effect chart of the project.**

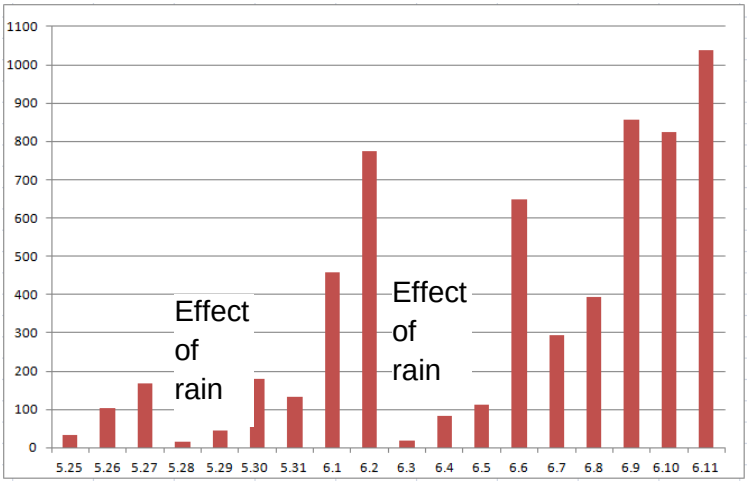

## 5.6 Quality analysis of seismic acquisition data of Yougou Block of Wuqi Oilfield

### 5.6.1 LVL (low velocity layer) investigation data

**Figure 39. Uphole interpretation result chart.**

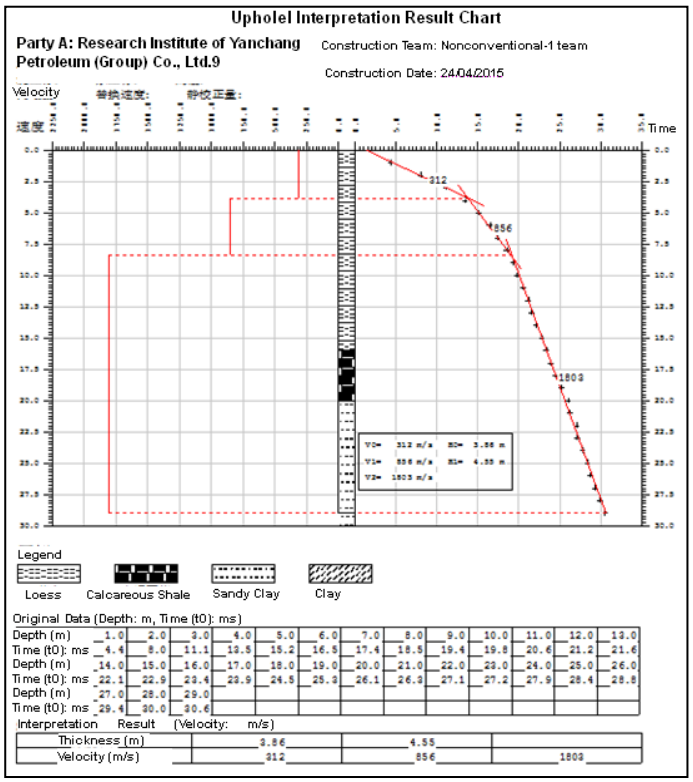


An investigation into the low velocity layer (LVL) was completed. To overcome the LVL, the standard procedure of using the Uphole seismic acquisition method was employed. Six Upholes (including two double Upholes) were designed and tested for accuracy and assurance. This included calculating the attenuation coefficient Q in data processing (See Figures 39 and 40). From analysis of LVL data and lithology from in the Upholes, the following result was obtained (Figure 40). The mountain area has complex topographic relief and the surface was covered by loess. The excitation conditions for seismic acquisition is poor and therefore the data quality is poor. The LVL is a wet loess layer with a thickness of about 0.8-2 m and lies about 6 to 10 meters in depth. Below the groundwater there is firmer, cemented layers with a layer thickness of about 1-3 m which lies about 8 to 17 meters in depth. This provides good excitation conditions with good quality acquisition.

**Figure 40. Uphole record.**

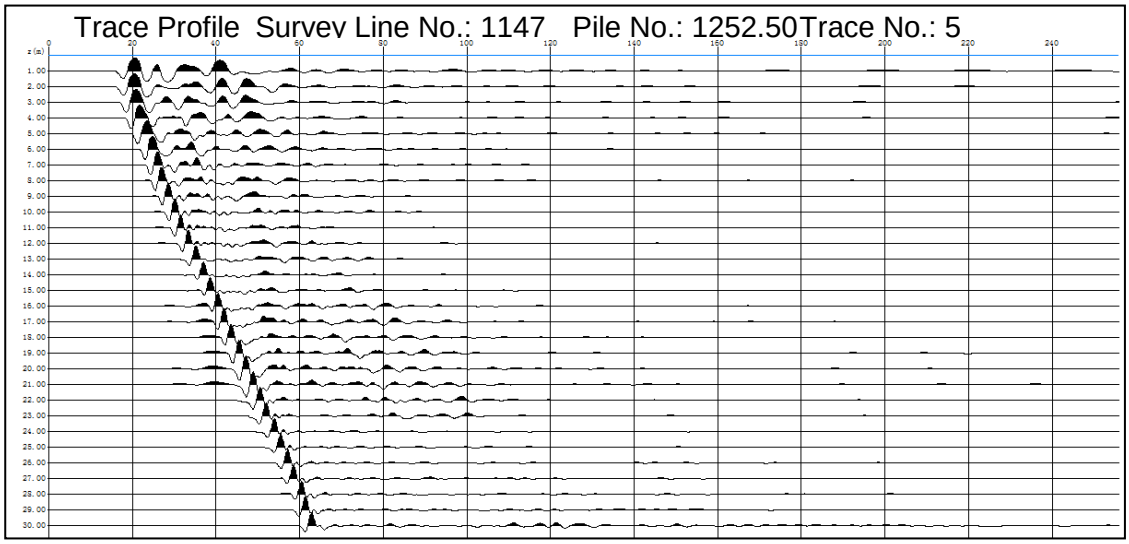


## 5.6.2 Double-Uphole

In double-Upholes the shotpoint is in one borehole, the receiver in the other borehole, both at the same depth (Figure 41). Because of this, when calculating the attenuation coefficient 'Q' make full use of the double Upholes' signal wave mechanics. The effect of different loess thicknesses which impact excitation energy consistency, absorption and attenuation resulted in the selection of the double-Uphole technique to investigate near-surface structures. There are six double-Upholes in this work area. See Figure 42 for the location and Table 17 for results and set up.

**Figure 41. Double uphole working Sketch Map**

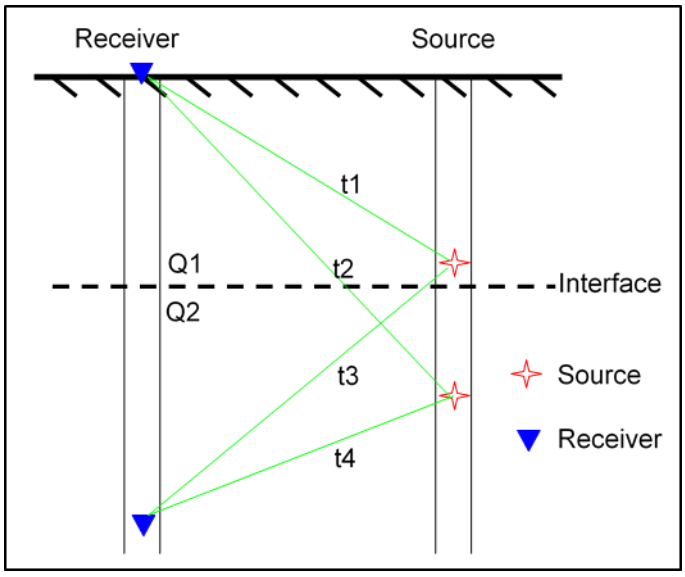


**Figure 42.Double-uphole Location Map. Yellow pins are double-uphole. (Source of base map: Google Maps).**

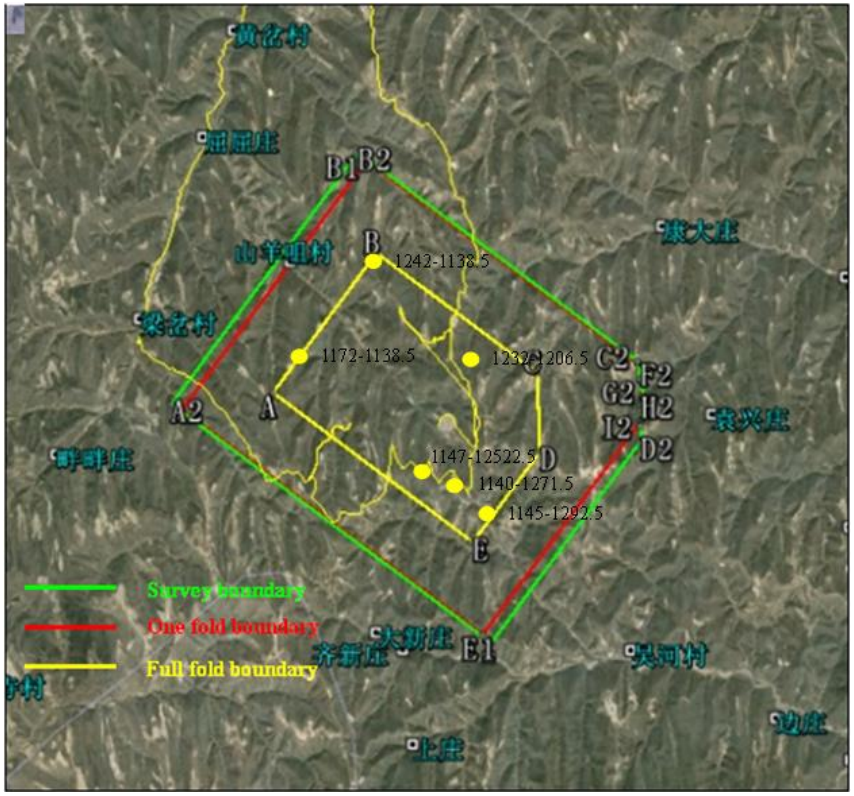
B1
B2
B
1242-1138.5
1172-1138.5
1232-1206.5
C2
F2
G2
H2
I2
D2
A2
A
1147-12522.5
D
1140-1271.5
1145-1292.5
E
E1
Survey boundary
One fold boundary
Full fold boundary

**Table 17. Double-uphole interpretation results.**

| | Survey Line No. | Pile No. | Elevation (m) | Water Table | h0 | h1 | h2 | H | V0 | V1 | V2 | V3 |
|---|---|---|---|---|---|---|---|---|---|---|---|---|
| | | | | Elevation (m) | (m) | (m) | (m) | (m) | (m/s) | (m/s) | (m/s) | (m/s) |
| **1** | 1,172 | 1,138.5 | 1,610.2 | 1,513.7 | 21.9 | 51.1 | 23.6 | 96.5 | 470 | 720 | 1,011 | 1,946 |
| **2** | 1,232 | 1,206.5 | 1,674.8 | 1,597.9 | 24 | 37.3 | 15.6 | 76.9 | 533 | 732 | 1,204 | 2,114 |
| **3** | 1,147 | 1,252.5 | 1,666 | | 14 | | | 14 | 448 | 612 | | |
| **4** | 1,242 | 1,132.5 | 1,600 | 1,519.5 | 13.1 | 30.8 | 36.6 | 80.5 | 440 | 662 | 1,321 | 2,104 |
| **5** | 1,140 | 1,271.5 | 1,493 | 1,484.6 | 3.9 | 4.6 | | 8.4 | 312 | 856 | 1,803 | |
| **6** | 1,145 | 1,292 | 1,549.7 | 1,507.5 | 12 | 30.2 | | 42.2 | 461 | 746 | 2,087 | |

### 5.6.3 Single shot data

The use of the Single Shot Method, which is the typical method of acquiring seismic, uses a source point in the borehole and receiver point on the ground. In this area, the Single Shot Data is used depending on different surface conditions, including loess-covered area and gully bottom. The excitation and reception conditions and the recorded geomorphologic features vary with surface conditions. In view of construction difficulties in this period, we used the Seismic Acquisition Site Management System (See Figure 43, seismic interpretation system from CNPC). This system uses the built-in GPS incorporating smart phone and electric compass assist in seismic acquisition. By introducing server management, the drilling, blasting, acquisition, supervision and pipeline cleaning modules enable real-time online data management and display of the whole process of seismic acquisition. This enables all operation teams to use the same set of data, allows the display of whole-process data attributes from the monitor client, and realises the real-time monitoring and quality control in the whole process of acquisition. This system has helped improve the drilling and blasting of shotholes punctuality. The deviation rate of the points in the whole area arising from drilling deviation, incorrectness of reported or marked pile number or any other reason found in the process of shot migration inspection is 0.8 per cent. The accurate design data statistics show that 6,177 shots are designed for this work area, 5770 in the loess-covered area, accounting for 93.4 per cent of total; 407 at the gully bottom, accounting for 6.6 per cent of total (See Table 18).

**Figure 43. Seismic QC monitoring system. Above map: Seismic acquisition progress map. Blue: recording points; Green: drilling points; Red: survey points.**

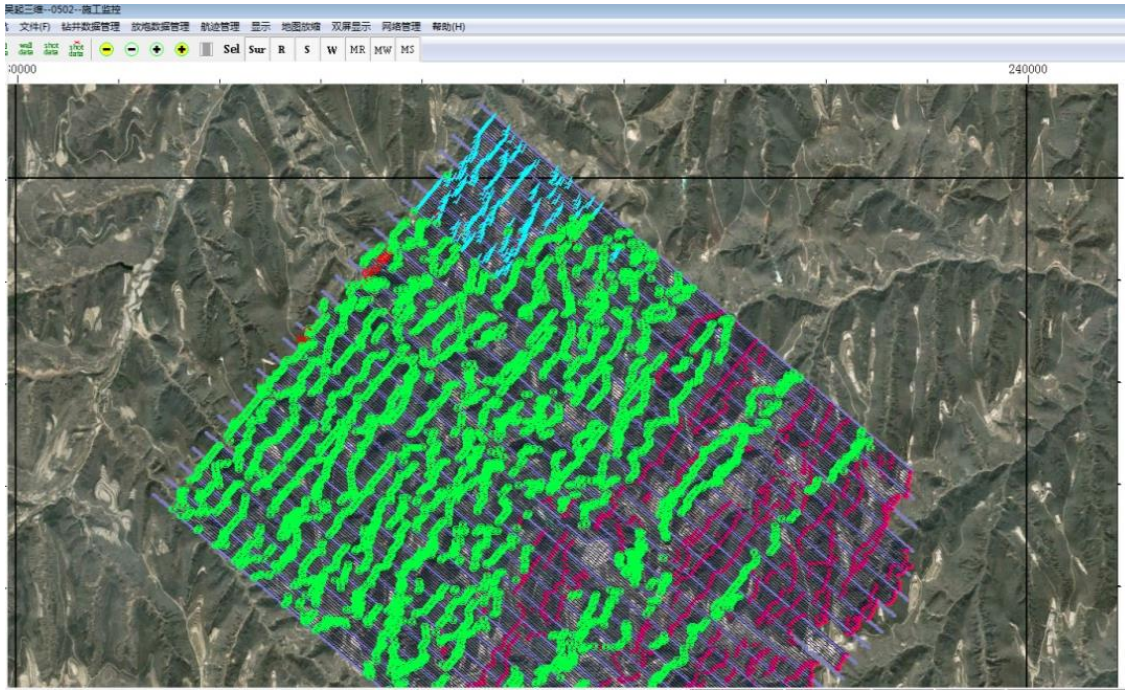


**Table 18. Statistics of shot points.**

| Landform | Number of Shots | Proportion |
|---|---|---|
| Loess-covered area | 5,770 | 93.4% |
| Gully bottom | 407 | 6.6% |

### 5.6.4 General record analysis

The whole area has distinct seismic wave group reflection features. The wave groups are characterised by strong energy and good continuity. The wave groups in Chang-4+5 reservoir in Triassic Yanchang Formation are continuously tracked in the whole area. From monitoring record and frequency-division scanning record, we can see that the gully bottom acquisition data has:

Comparable quality across the area:

- strong energy record
- resolution and SNR are high
- target reservoir is clear
- continuity is good
- advantageous bandwidth is 0-80Hz
- basic frequency is about 36Hz.

Due to bad surface excitation and receiving conditions and weak energy, the record of the loess-covered area gives moderate SNR and low frequency.

**1. Analysis of loess-covered area data**

The excitation conditions are neither good nor bad, due to the poor conditions. Figure 44 is typical record of a loess-covered area, showing strong recorded energy and very continuous target stratum as tested by single-shot record. In part of the loess-covered area where the excitation points are close to the buildings or structures like water cellars, oil production stations and caves, the charge size is often reduced to an appropriate amount for the purpose of safety. Compared with normal recorded energy, the recorded energy obtained from these places is weaker and the continuity is a little worse, but the frequency is at a similar level.

**Figure 44. Typical record of tableland.**

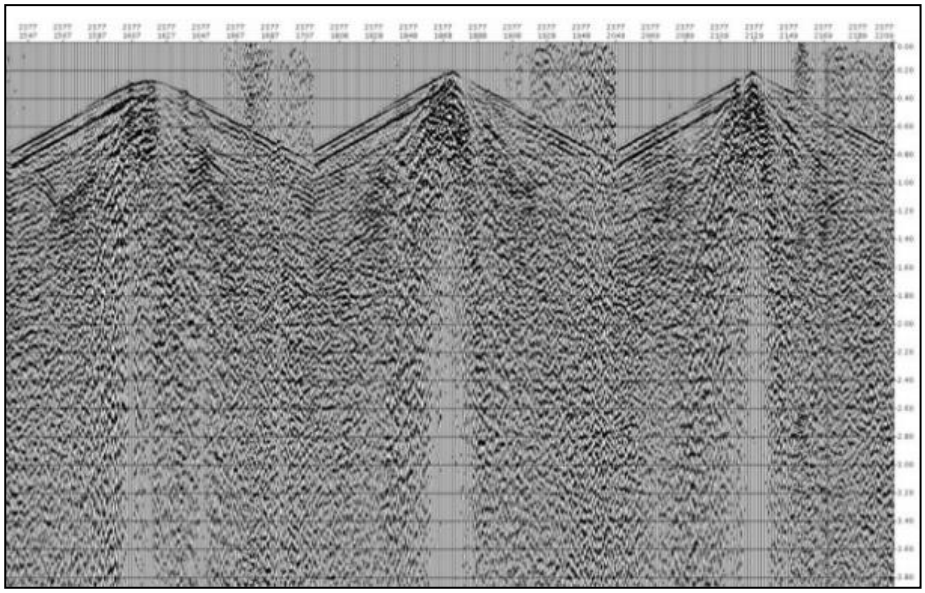

**Figure 45. Typical record of gully.**

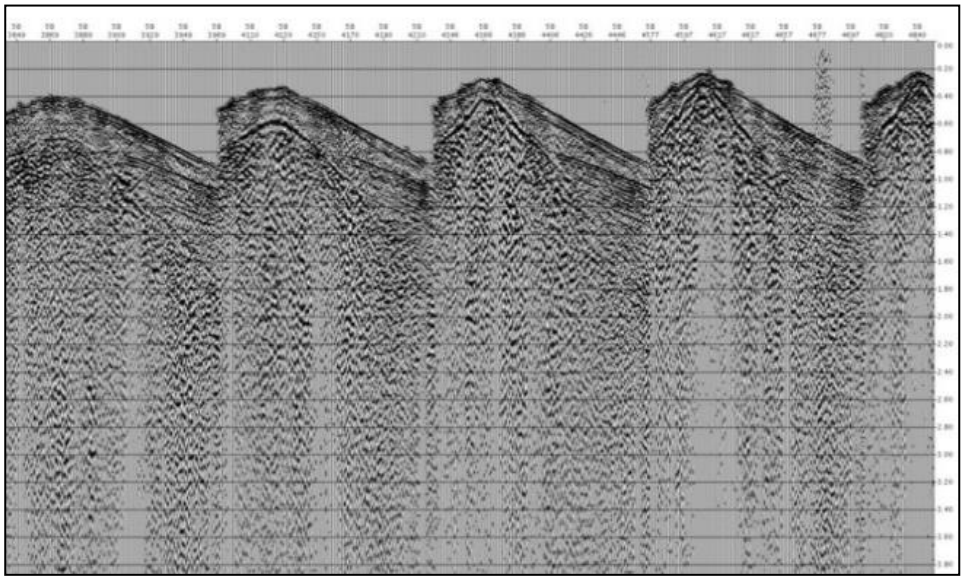

**2. Gully data analysis**

The gully bottom data shows good quality and high SNR. The reflected wave groups in the major target interval are complete and have obvious features, good continuity and high visual frequency as well as fewer abnormal traces but strong recorded energy. The reflected wave groups in the target stratum of effective reservoir are distinguishable and have strong effective wave energy and good continuity. Figure 45 is typical record of gully, showing good record quality and strong energy.

### 5.6.5 Analysis of interference source

Major sources of interference to this work area are the interference from oil production stations, the interference from motor vehicles and background interference.

**1. Interference from oil production stations**

There are many oil production stations on the loess tableland and they are a great interference to the seismic acquisition process (Figure 46). This type of interference features fixed interference sources and strong interfering energy. Moreover, when the recorded energy is weak during acquisition, this interference has an even larger impact on the recorded energy. The major interference exerted by oil production stations is dynamic interference from pumping unit motors. In this case, the radius of interference is usually 100-150m and the effect on record usually involves 3 to 4 lines, and each line could further affect 5 to 8 traces. As the pumping units work on a 24-hour basis, certain records are affected to a certain extent.

**Figure 46. Record of interference from oil production stations. (Left-original record. Right-filtered record).**

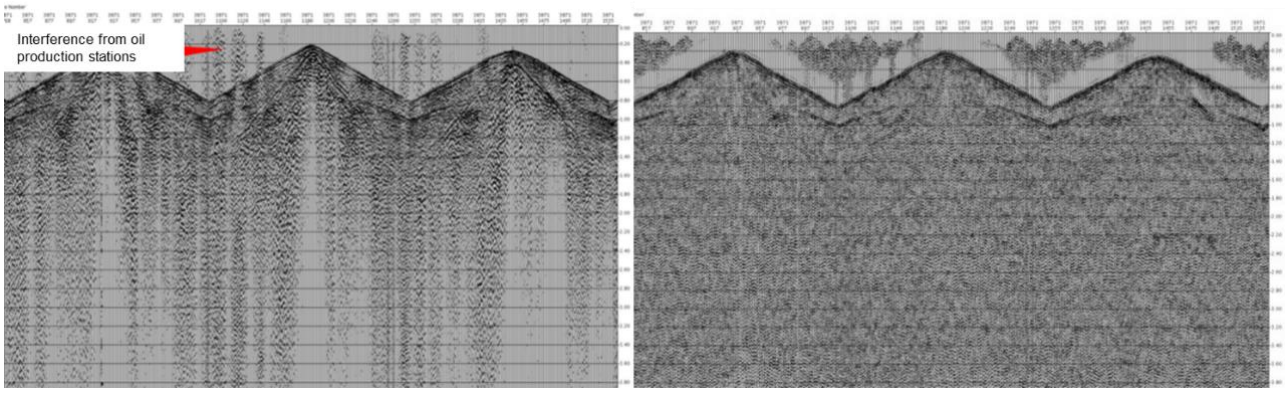


**2. Interference from motor vehicles**

There are many roads in the work area and vehicles use the roads day and night, including construction machinery to serve the oilfield. Although some precautionary measures are taken, vehicle interference is record in some instances. Figure 47 is a typical record of interference from motor vehicles in the work area. The interference signals from oil tankers have strong energy and low frequency. A large portion of this interference can be eliminated by filtering, but the rest still has some effect on the data.

**Figure 47. Record of Interference from Motor Vehicles. (Left-original record. Right-filtered record).**

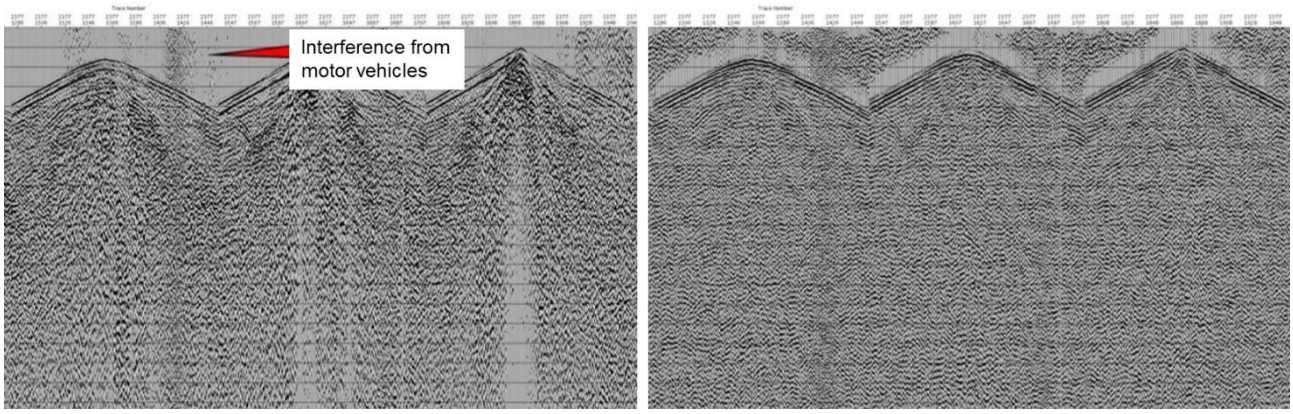


### 5.6.6 Analysis of interference wave

Based on the single shot obtained in this test, the interference wave of this work area is show in Figure 48.

**Figure 48. Interference wave investigation.**

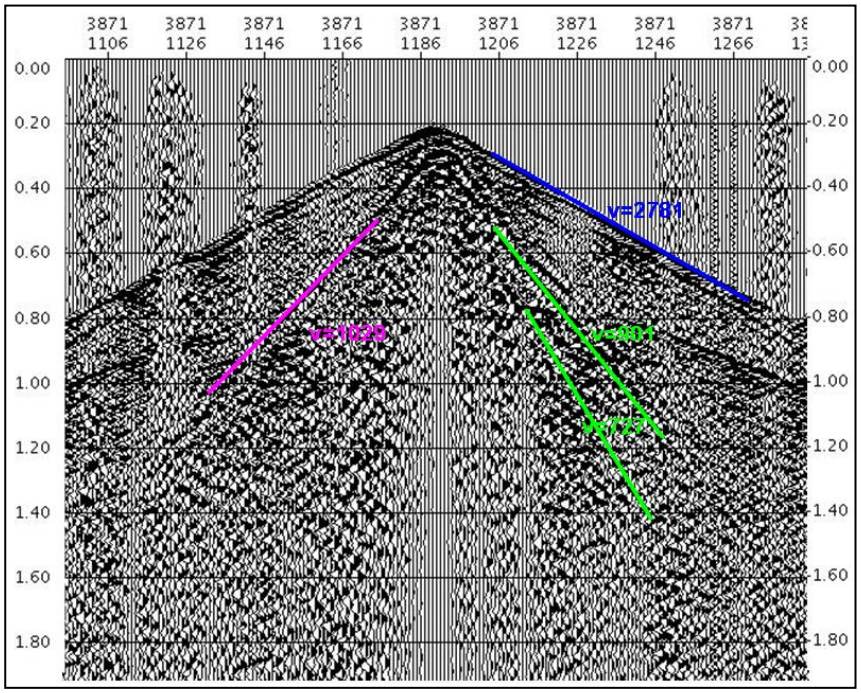


From the analysis of interference wave (Table 19), comparing the interference wave frequency received, it was concluded that the data quality in this area is the largest of the refraction wave, and it is strong, with a wide frequency band. This seriously affects the objective layer.

**Table 19. Major parameters of interference wave in work area.**

| Type of Interference Wave | | Visual Velocity (m/s) | Visual Frequency (Hz) |
|---|---|---|---|
| Surface wave | Surface wave 1 | 700-750 | 6-15 |
| | Surface wave 2 | 850-950 | 10-20 |
| | Surface wave 3 | 1000-1050 | 13-25 |
| Refracted wave | Refracted wave 1 | 2750-2800 | 22-42 |

## 5.7 Observation system inspection and analysis

The accuracy defined by the observation system was inspected by several technical approaches, such as layout plans of shot and inspection points and linear dynamic correction.

In this work area, there are a large number of obstacles, including houses, graves, caves, oil production stations and water injection stations and gas injection stations. As many shot points are needed, their positions were corrected, resurveyed or offset to another location (See Figures 49 and 50).

**Figure 49. Geometric inspection.**

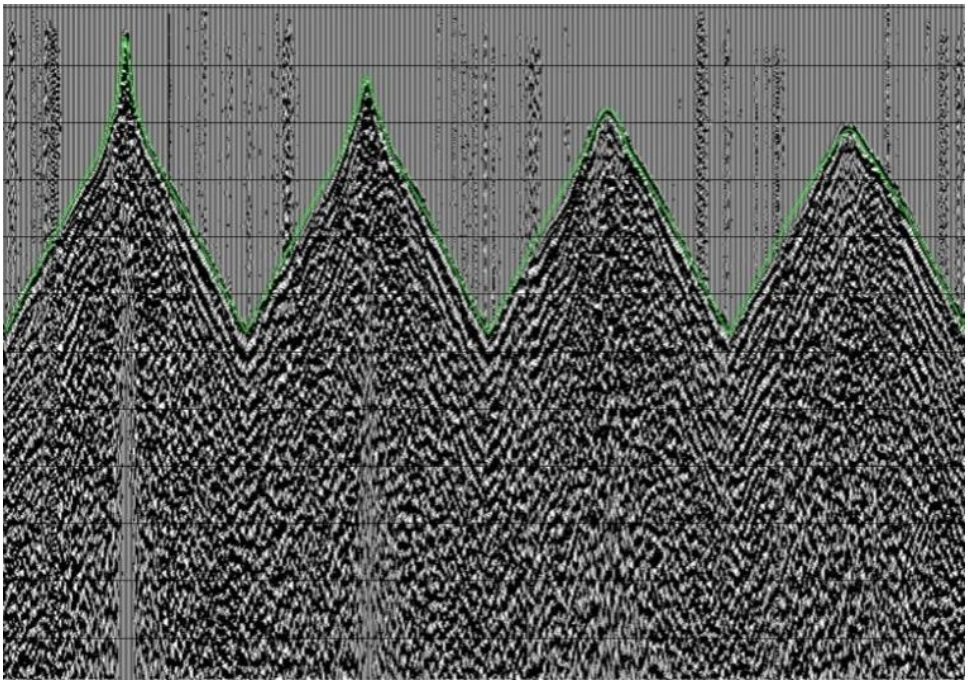

**Figure 50. Offset distance and Azimuth analysis (left) and fold analysis (right).**

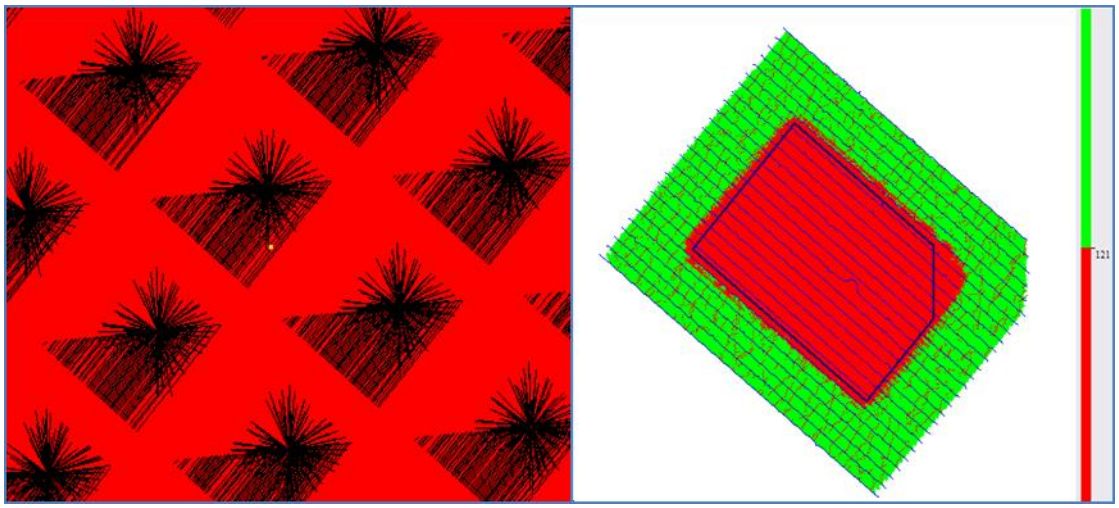

### 5.7.1 Static correction

This work area is characterised by ragged topography, complicated surface and significant difference in thickness and velocity of weathered/sub-weathered layer. Therefore, the resolution of the static correction problem is vital to improve the processing effect. For this work area, the elevation static correction and tomographic static correction were applied in field monitoring and processing. This practice achieved a good effect.

The ragged topography and uneven distribution of thickness and velocity of weathered/sub-weathered layer in this work area lead to the severe influence on stacking effect and the reduction of basic reflection frequency and profile SNR. For this reason, the properness of static correction is directly related to the profile effect. Here is the result of comparison of single-shot record before and after tomographic static correction.

From it, we can see that the continuity of wave groups has a significant change after correction (See Figure 51).

**Figure 51. Effect of topographic static correction: before correction (left) and after correction (right).**

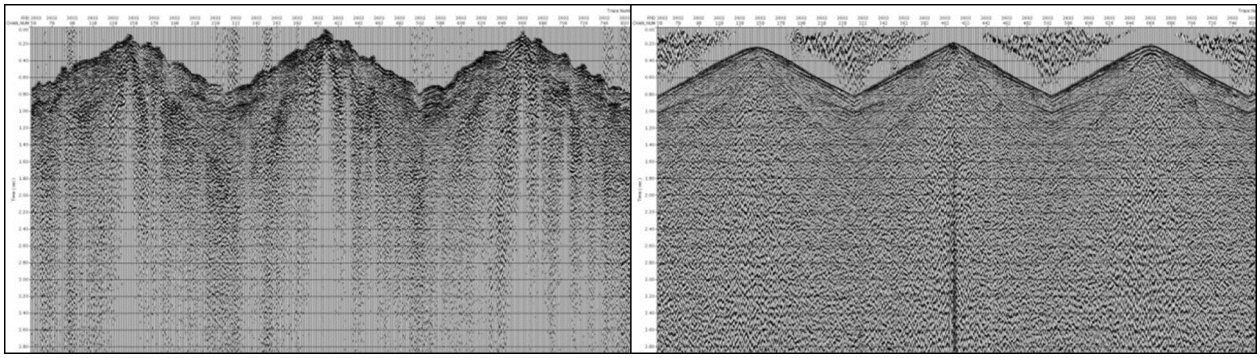

## 5.7.2 Velocity analysis and dynamic correction

The development of surface waves in this work area resulted in the scattering of energy groups of each wave group. The strong energy of refracted wave and multiple refracted wave has seriously affected the selection of wave group velocity. To solve this problem, the band-pass filtering and first arrival muting techniques were used in the monitoring and processing of this work area. In this way, surface wave, refracted wave and multiple refracted wave can be effectively inhibited. This allowed the energy group of effective wave group to be displayed in a more intensive manner, so that velocity can be selected more accurately.

The dynamic correction of the shot record against the velocity determined in velocity analysis was made. Then, the results were transformed into the self-excitation and self-receiving shot record. The record obtained was processed by stacking to generate the initial seismic profile. This profile was processed by residual static correction to get the final field monitoring profile.

## 5.7.3 Profile data

The field monitoring profile shows that this area has continuous characteristic wave group with high resolution and SNR. It reaches the design requirement of 3D seismic acquisition.

From the field stacking profile, Yan-2 and Chang-7 are two clear seismic responses that reflect sedimentary rock layers. Both Yan-2 and Chang-7 have good continuity, strong energy and high SNR; they are easy to identify and track and have obvious structure. This profile also shows that the reflected wave in shallow, intermediate and deep layers has high SNR; major exploration target features large reflection strength, energy balance and good continuity as well as clear geological structure and rich interlayer information. In conclusion, an ideal exploration effect was achieved.

**Figure 52. Seismic section: Layer information (Red line: Yan 1 to Yan 6, Blue line: Chang 7)**

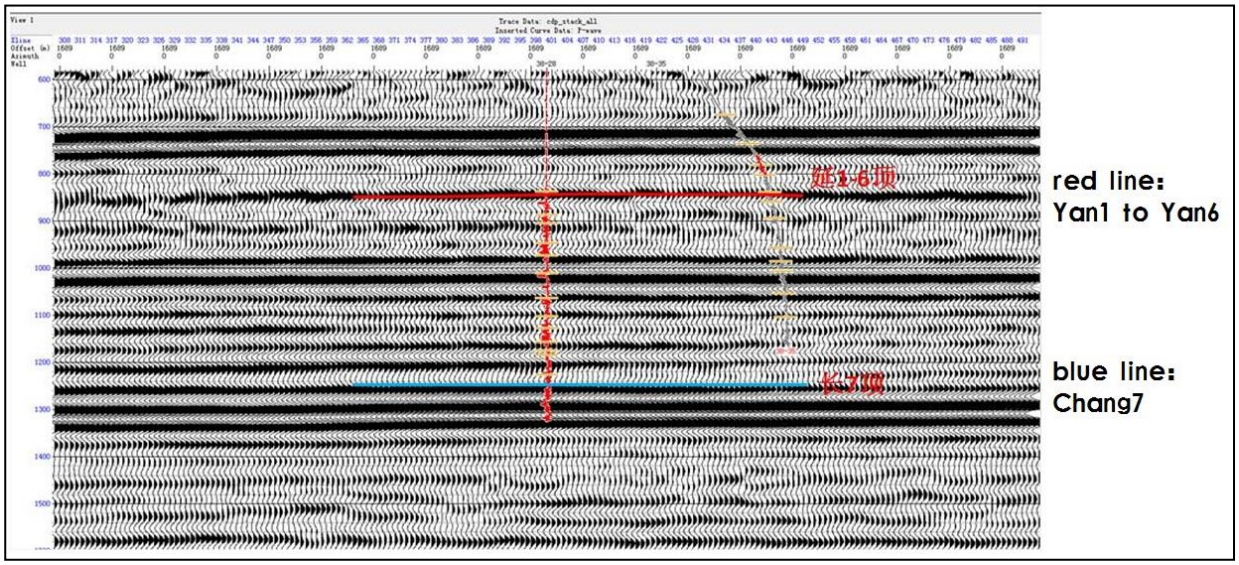


The profile frequency-division scanning results show that the effective reflection energy is strong and that the wave group continuity is good at 20-40Hz and 30-60Hz (See Figures 52 to 59); note: the three colours (yellow, red, blue) in the figures mark three strong reflectors created by the analysis software which can be adjusted freely, does not represent information of layer. It is difficult to determine the relationship among the three reflectors and the layer.

**Figure 53. Inline 100CMP profile and spectral analysis-3 windows are different rock layers.**

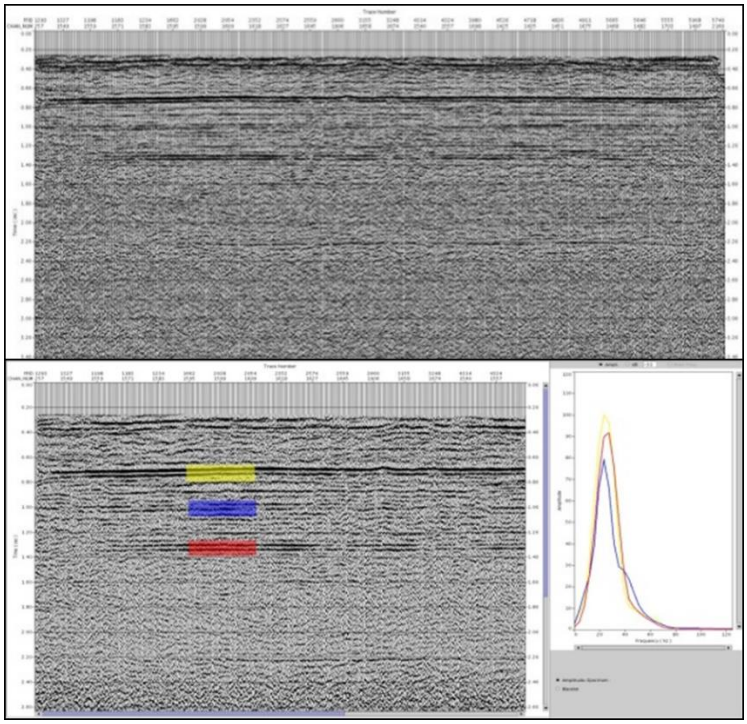

**Figure 54. Seismic section: Inline 150CMP profile and spectral analysis-3. Three obvious reflectors can be seen. The graph is the spectrum analysis curve corresponding to three reflectors.**

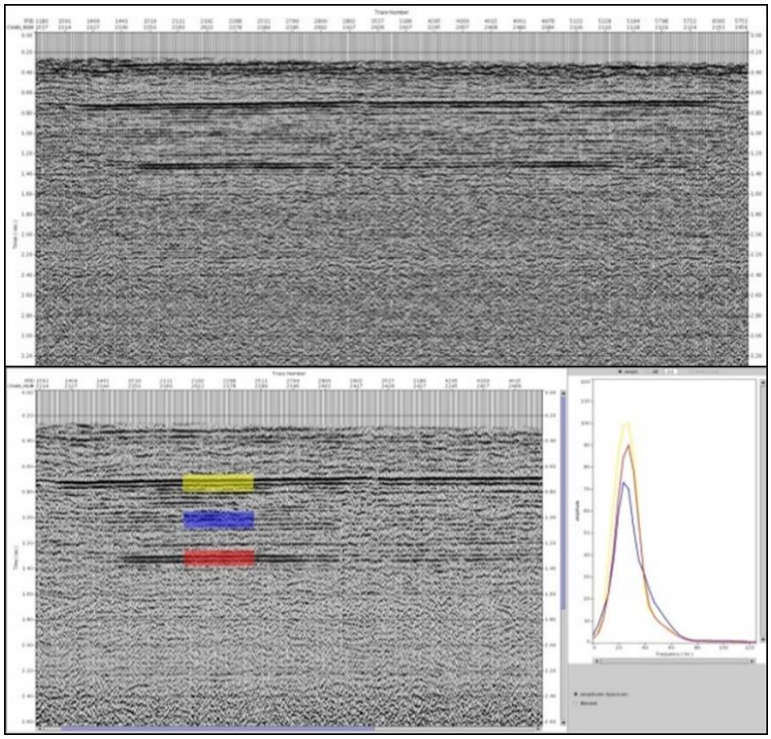

**Figure 55. Seismic section: Inline 200CMP Profile and spectral analysis-3 windows are different layers. The graph on the right side of the figure is the spectrum analysis curve corresponding to three reflector.**

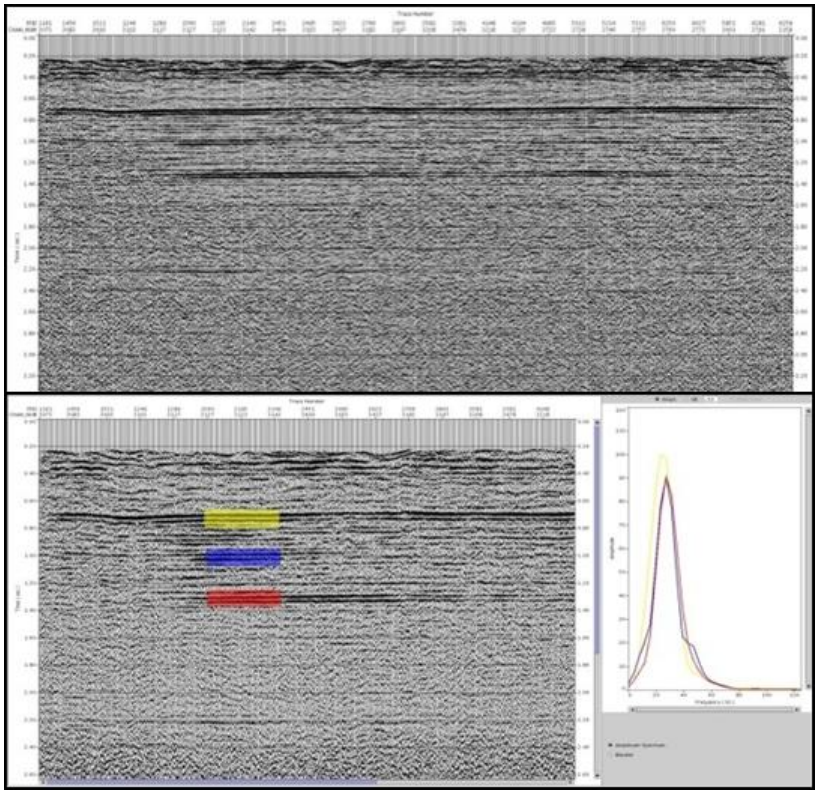

**Figure 56. Seismic section: Inline 250CMP Profile and spectral analysis-3 windows are different layers.**

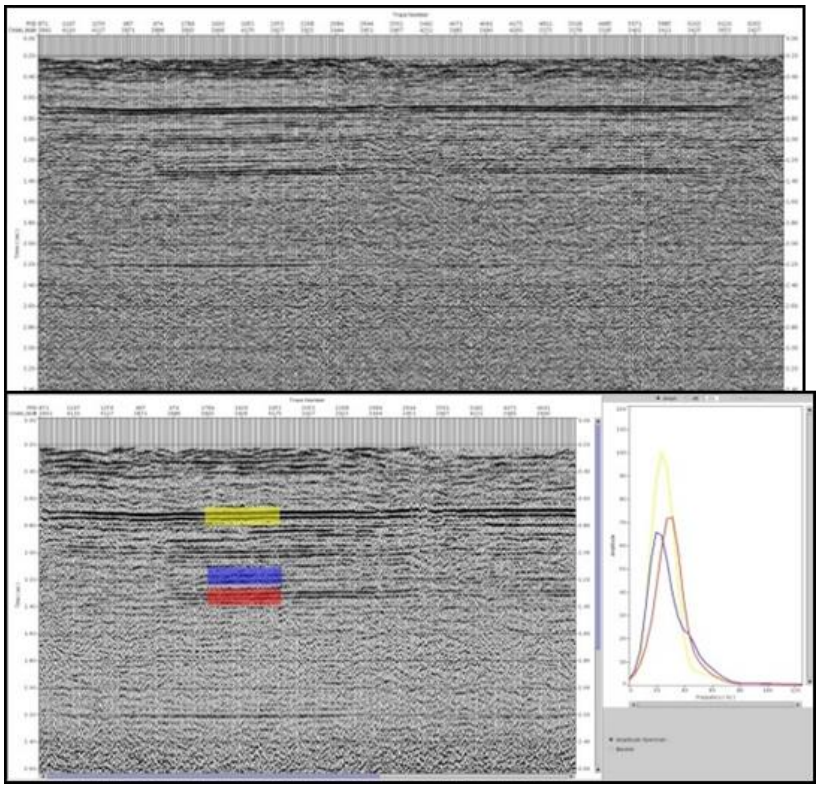

**Figure 57. Seismic section: Inline 300CMP profile and spectral analysis.**

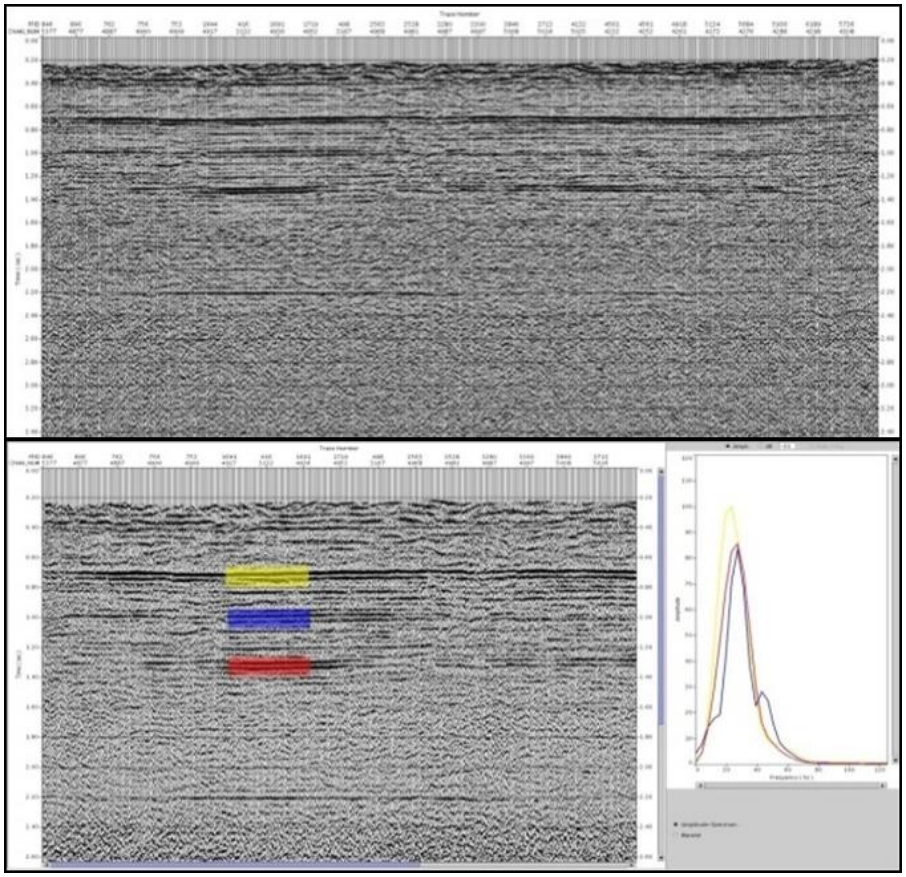

**Figure 58. Seismic section: Inline 100CMP Profile at fractional frequency of 10-20Hz (left) and Inline 100CMP profile at fractional frequency of 20-40Hz (right).**

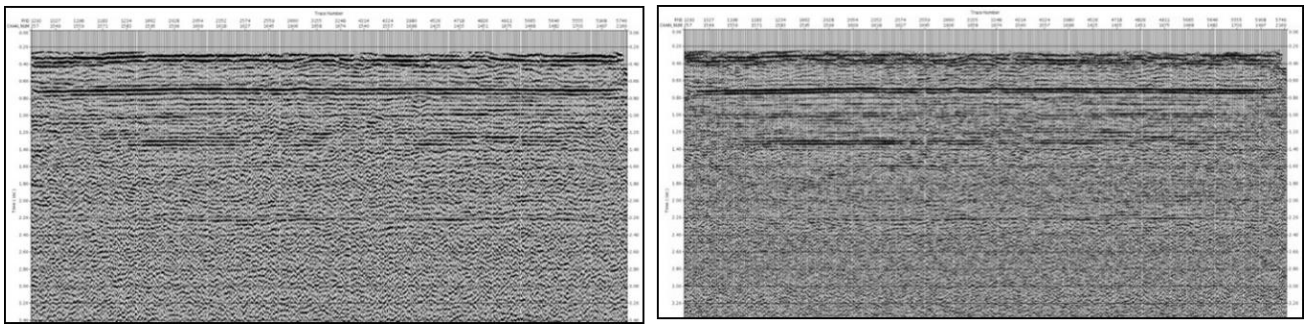

**Figure 59. Seismic section: Inline 100CMP Profile at fractional frequency of 30-60Hz (left) and Inline 100CMP profile at fractional frequency of 40-80Hz (right).**

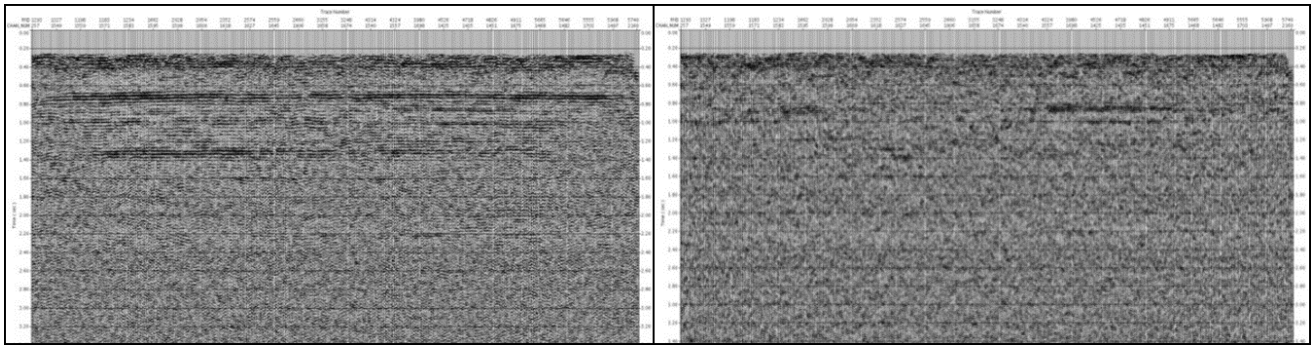

**Figure 60. Seismic section: 0-1500m Offset Profile (100CMP) (left) and 1500-4,000m Offset Profile (100CMP) (right).**

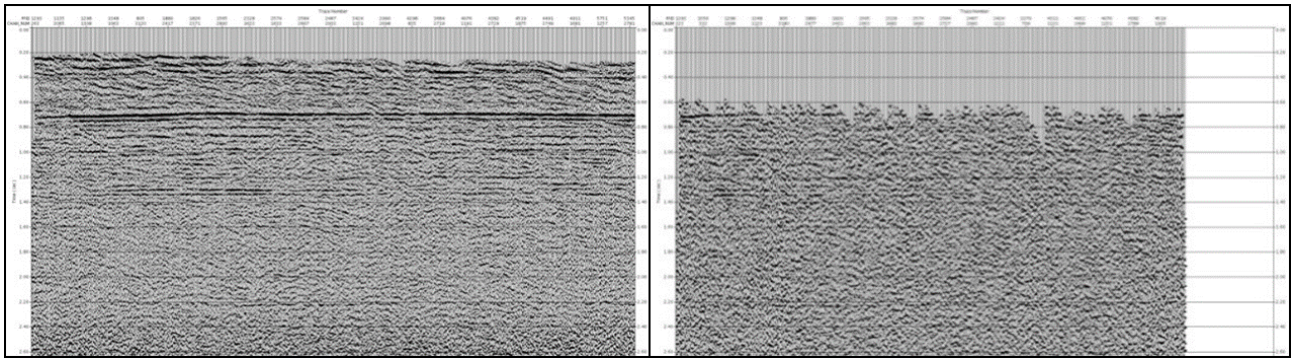

The spectral analysis of each target stratum in the stacked profile finds that the basic frequency of each layer is about 30Hz and the bandwidth is 10-65Hz. From the above near and far offset profiles, we can see that the target stratum in the near-offset profile is continuous and each stratum is complete. From the far-offset profile, we can see that Yan-2, Chang-7 and base have effective information.

# 6 Planned monitoring and verification program

In addition to current monitoring activities, Yanchang Petroleum will further improve the sequestration monitoring. The next step monitoring plan can be divided into four parts (As shown in Table 20).

**Table 20. MMV techniques and technologies planned for research area.**

| Environment | Method | Technology/Technique |
|---|---|---|
| **Atmosphere** | Near-surface atmospheric sampling | $CO_2$ and xenon gas content using:<br>portable infrared $CO_2$ concentration detectors<br>surface $CO_2$ concentration detectors |
| **Surface/Subsurface** | Surface deformation | Interferometric synthetic aperture radar (InSAR) |
| | Water sampling | pH value, electric conductivity, TDS, carbonate content, bicarbonate content and heavy metal content |
| | Soil testing | LI-8100 automatic soil carbon flux measuring system<br>C13 isotope analyses |
| **Well** | Well monitoring | Corrosion monitoring<br>electromagnetic defectoscope |
| **Reservoir** | Well measurement | Tracer |
| | | Downhole pressure and temperature |
| | Well geophysics | Cross-hole seismic |

## 6.1 Above ground monitoring

Above ground monitoring is primarily real-time detection of surface air concentration. The method of monitoring the ground-level concentration of $CO_2$ is to effectively monitor the $CO_2$ concentration by fixed-point, continuous or fixed-time sampling and measurement of $CO_2$ in the atmosphere within certain scope (the near-surface zone of the $CO_2$ capture area and sequestration area). To monitor the concentration and flow of $CO_2$ in air, the common practice is to set several $CO_2$ monitoring points near the injection site and within kilometres away from it. Then, the continuous automatic monitoring is conducted by stationary or on board automatic monitoring equipment, and relevant data acquired is sorted and analysed. Additionally, portable infrared gas analysers or $CO_2$ alarms are provided, so that people can take emergency measures in case of emergency (eg, $CO_2$ leakage).

Above ground monitoring is being conducted both in Jingbian and Wuqi sites using portable $CO_2$ concentration detectors and near-surface $CO_2$ concentration detectors to determine the real-time concentration of air-borne and near-surface $CO_2$ since prior to injection and during the injection monthly, and will monitor for a long time until the end of the project. The goal of the above ground monitoring systems is to identify $CO_2$ leakage during injection operation. Before using this method, the background value of $CO_2$ near wellhead will be established. Atmospheric $CO_2$ concentration, atmospheric temperature, cloud cover, wind velocity, wind direction, relative humidity, and pressure will be measured and monitored. The purpose is to monitor the potential escape of $CO_2$ from the sequestration site and provide basic data for environmental safety impact assessments of the sequestration project. The biggest challenge comes from the uncertainty of the leak point, In that case, more and more advanced monitoring methods will be implemented during the project operation.

## 6.2 Surface monitoring

Proposed surface monitoring items include soil carbon-13 isotope, shallow soil flux, surface water and surface change. Soil carbon-13 isotope monitoring and shallow soil $CO_2$ flux monitoring are two ways to reflect the leakage of sequestrated $CO_2$. The surface water monitoring is to monitor the composition and quality of surface water for a long time, and it helps us know the effect of $CO_2$ sequestration on surface water. By monitoring surface changes, we can study the physical changes of the surface after $CO_2$ sequestration.

### 6.2.1 Shallow soil $CO_2$ flux

Soil gas analysis is a good method for near-surface $CO_2$ monitoring. Sampling and analysing the $CO_2$ gas in the soil layer makes it easy to effectively monitor if $CO_2$ leaks into the soil. The advantage of this method is the sensitivity to slight $CO_2$ leakage. Soil $CO_2$ flux is subject to multiple complex physical and biological processes in time and space. It is planned to use LI-8100 automatic soil carbon flux measuring system for long-term, continuous and accurate measurement of soil carbon flux. This system can realise independent long-term monitoring and short-term measurement. The long-term measuring chamber has the function of automatically monitoring the daily change of soil $CO_2$ flux from the same position for as long as several months. The short-term measuring chamber has the function of quickly measuring the soil $CO_2$ flux, acquiring the data from different positions and fulfilling the accurate determination in different spatial scales.

This monitoring will take place in both Jingbian and Wuqi. Before $CO_2$ injection it did not monitor the shallow soil $CO_2$ flux, so it is planned during $CO_2$ injection and monthly intervals. It is also planned to continue monitoring after the cessation of $CO_2$ injection. The primary reason for this analysis is to ensure that the soil $CO_2$ flux during $CO_2$ injection obtained from all points are similar to the background soil $CO_2$ flux values in area without $CO_2$ injection. This can assist in safety impact assessments and in identifying the source of potential high $CO_2$ measurements.

### 6.2.2 Soil carbon-13 isotope monitoring

The main method for monitoring the carbon-13 ($\delta^{13}C$) isotope in soil gas is to sample the $CO_2$ gas in the near-surface soil layer (1-2m). The samples will be assayed to calculate the content of $\delta^{13}C$ stable isotope of $CO_2$ gas in the sample in the laboratory and trace the source of $CO_2$. Generally speaking, the value range of the $\delta^{13}C$ isotope already existing in soil is different from that of the injected $\delta^{13}C$. The advantage of this method is the sensitivity to slight $CO_2$ leakage, even though the challenge is that the soil carbon-13 isotope sample is difficult to collecting. This monitoring will take place in both Jingbian and Wuqi and was completed prior to injection and during $CO_2$ injection at yearly intervals. The plan is to do this monitoring after $CO_2$ injection finished. Through comparison of monitoring and assay results, the isotopic signature can be identified if the injected $CO_2$ has spread to the surface soil that will lead to the implementation of proper measures to prevent the further escape of $CO_2$ to the atmosphere and attain the goal of monitoring and early warning of $CO_2$ leakage.

### 6.2.3 Surface water and shallow groundwater monitoring

In this region, most of the potable water and water for agricultural purposed are from surface water, including dams. So, the safety of surface water as well as the groundwater is vital. The monitoring of $CO_2$ content of these water sources in the sequestration area aims to identify if there is leakage of sequestrated $CO_2$. This is achieved by comparing the $CO_2$ content through gas sampling of the surface water before and after $CO_2$ injection. This method is to use the water quality fast-test system both onsite and in the lab. Measurement of the water will be below parts-per-million levels, ensuring levels do not exceed the background data prior to

injection of $CO_2$. The purpose is to monitor the pH value, electric conductivity, TDS, carbonate content, bicarbonate content and heavy metal content of surface water and groundwater existing in the monitoring area and around; check abnormal points and find possible leakage. This monitoring will take place in both Jingbian and Wuqi. Sampling has taken place prior to injection, and then will continue during $CO_2$ injection at yearly intervals as well as after injection.

### 6.2.4 Interferometric synthetic aperture radar (InSAR) monitoring

Synthetic Aperture Radar (SAR) is a high-resolution 3D imaging radar. In the last 20 years, great progress has been made in this brand new air-to-land observation technology. It has grown to an essential remote sensing tool. With this technology, changes in the landscape can be measured across environments and identify debris-flow deposition, delta evolution and movement of great sand dunes. It also allows the measurement of slight physical movement occurring on the surface at the radar wavelength level. The purpose is to quantitatively monitor the surface deformation caused by $CO_2$ injection and oil and gas production and the effects of $CO_2$ plume movement. This surface deformation could have consequences for the environment and safety risks of the strata above the reservoir and the surface infrastructure. Currently, Yanchang is not doing this monitoring, but plan to do applied research on how to implement the technology.

## 6.3 Subsurface monitoring

Proposed surface monitoring items include cross-hole seismic monitoring, gas tracer monitoring and stratum pressure monitoring. The cross-hole seismic monitoring is to monitor the migration and distribution of $CO_2$ between wells. The gas tracer monitoring will enable the migration of the plume to be identified and will offer insight into the connectivity between reservoirs and surrounding strata or between fault blocks.

### 6.3.1 Cross-hole seismic monitoring

A rich diversity of techniques is available for subsurface monitoring, including cross-hole seismic monitoring, micro-seismic monitoring and time-lapse seismic monitoring. These techniques have become a mature application in many CCS projects. Cross-hole seismic monitoring will obtain cross-hole geological profile by exciting seismic wave from a seismic source down a well, receiving the seismic wave from a geophone in another well, and systematically processing the seismic records. As it avoids the surface weathered (or low-velocity) layer which may absorb the high-frequency component of seismic signals, it can be used to obtain seismic signals with very high resolution. In this way, the extremely precise imaging of geological targets (eg, cross-hole stratum, structure and reservoir) can be obtained.

In most cases, the cross-hole seismic monitoring technology is applied to study the continuity of cross-hole stratum, grasp the lateral changes of reservoirs, describe oil reservoirs and monitor the dynamic status of oil and gas reservoirs. It can also be applied to:

- obtain the details of underground geological structure
- provide the anisotropy data and describe oil reservoirs
- observe barriers in faults and sedimentary units, the boundary and horizontal and cross bedding between sedimentary units, the permeable zone and fracture development degree of sedimentary units, etc
- lithology identification and EOR monitoring.

If the cross-hole migration and distribution of $CO_2$ is monitored by the cross-hole seismic technology before and after gas injection, we a good understanding of sequestration conditions can be reached. Yanchang

Project is planning on conducting cross-hole seismic monitoring in the two sites Jingbian and Wuqi. This monitoring will take place through injection and production wells.

### 6.3.2 Gas tracer monitoring

There are two types of gas tracers, radioactive tracer and chemical tracer. Chemical tracer has replaced radioactive tracer which are used to occupy the leading position in miscible displacement. Among chemical tracers, perfluorocycloalkane and sulphur hexafluoride have been widely tested and applied on site. This technology is applied for tracer monitoring of the water-alternating-gas (WAG) miscible- displacement oilfields, and it has achieved a good results. Yanchang Project is planning on conducting this monitoring in the two sites Jingbian and Wuqi through a cooperative project from CAGSIII (China Australia Geological Storage of $CO_2$ Project). Technologies including U-tube in monitoring wells will be completed at Yanchang by this cooperative project. The purpose of this technique is to monitor the $CO_2$ migration by co-injecting $CO_2$ with other compounds into the target reservoir. Through gas tracer monitoring, the velocity and motion direction of injected gas can be measured and it enable the injected gas breakthrough time and the connection between injection wells and neighbouring monitoring wells. The results of tracer monitoring will not only identify preferential migration channels, but also the connectivity between strata and/or fault blocks. This data can then be used to correct the original oil reservoir model in order to select the optimum production mode.

### 6.3.3 Stratum pressure monitoring

Stratum monitoring is primarily to track and monitor underground $CO_2$ migration, measuring the:

- porosity, permeability and saturation of each $CO_2$ reservoir
- temperature and pressure of each reservoir/caprock
- chemical reaction with the reservoir, $CO_2$ front position, pressure distribution, corrosion to casing, etc.

Among all monitoring items, the most important is pressure. During execution of the CCS project, the stratum pressure will be monitored at all times. This will prevent the fracture of the reservoir and caprock under the action of $CO_2$ pressure build up, known as the fracture pressure, which could occur if the fracture pressure is exceeded. If the pressure escalates and the fracture pressure is exceeded, it may produce a fissure or minor fault which could create an opportunity for $CO_2$ to move beyond the reservoir. This monitoring will take place in both Jingbian and Wuqi. Pressure monitoring will occur throughout the injection operation in both production and injection wells. The purpose of the monitoring is to monitoring the reservoir/caprock pressure in situ including the real-time monitoring of injected $CO_2$ migration and diffusion. Through comparative analysis of the change of stratum pressure before and after gas injection, a loss of pressure could mean $CO_2$ leakage that can then be rapidly addressed.

### 6.3.4 Well condition monitoring

The well borehole will be tested and analysed for integrity by using hole-diameter flaw detection. This is to monitor the damage of casings after $CO_2$ injection and investigate the impact of $CO_2$ on the casings of injection wells and oil production wells. The hole-diameter flaw detector will monitor the well conditions by means of electromagnetic defect scope to detect potential cracks and openings on a drill string. After calculation of current wall thickness of string, the corrosion status of the downhole string can be compared. The monitoring purpose is to monitor the damage (crack, corrosion, etc.) of casings after the $CO_2$ injection and to investigate the impact of $CO_2$ on the casings of injection wells and oil production wells by means of hole-diameter flaw detection. The wells in the Yanchang fields are the main $CO_2$ leakage point direct to the atmosphere, so it is very important to do the well condition monitoring to insure the completion of well hole.

# 7 Calculation of $CO_2$ sequestration capacity

The CSLF (2007) details the sequestration mechanisms. These mechanisms are divided into two broad types: physical sequestration and chemical sequestration. For $CO_2$-EOR in oil reservoirs, the specific mechanisms include:

- physical sequestration: free phase gas and residual
- chemical sequestration: dissolution mechanism and mineralisation.

## 7.1 Assessment of $CO_2$ sequestration potential of the Yanchang Oilfield

The sequestration potential of Yanchang Oilfield was assessed. In total, 176 oil reservoirs in Yanchang Oilfield were classified across two types: reservoirs suitable for immiscible displacement or reservoirs not suitable for immiscible displacement (Table 21). The system software assessing the sequestration potential of Yanchang Oilfield was developed by Yanchang Petroleum. The outcomes from this study are comparable to the results of Shaanxi Yanchang Petroleum (2015) report.

**Table 21. Screening Criteria of Oil Reservoirs for $CO_2$-EOR.**

| Screening Item | | Miscible Displacement | Immiscible Displacement | Depleted Oil Reservoir | Corresponding Factor |
|---|---|---|---|---|---|
| Crude oil Property | Crude oil gravity (°API) | >25 | >11 | >11 | Miscibility |
| | Crude oil viscosity (mPa.s) | <10 | <600 | | Miscible characteristics and injectivity |
| | Crude oil composition | High content of C2 to C10 | - | - | Miscibility |
| Reservoir Feature | Oil reservoir depth (m) | 900~3000 | >900 | >900 | Miscibility |
| | Average permeability (md) | N/A | - | - | Injectivity |
| | Oil reservoir temperature (℃) | <90 | - | - | Miscibility |
| | Oil saturation (%) | >30 | >30 | - | EOR potential |
| | Coefficient of variability | <0.75 | <0.75 | - | Sweep efficiency |
| | Ratio of longitudinal permeability to transverse permeability | <0.1 | <0.1 | - | Buoyancy effect |

| | | | | | |
|---|---|---|---|---|---|
| | Horizontal permeability ($m^3$) | >10-13~10-14 | >10-13~10-14 | - | Injectivity |
| | Oil saturation | >0.05 | >0.05 | - | Sequestration capacity |
| | Oil reservoir pressure (MPa) | Initial injection | Injection after water flooding | - | Miscible condition |
| | | Initial pressure (Pi) >estimated minimum miscibility pressure (MMP) | Current Pressure (Pcurrent)>MMP | | |
| Caprock Feature | Sealing performance of caprock | Fracture is not developed on the caprock. | | | Safety |

According to Table 21, the statistics of about 176 oil reservoirs in Yanchang Oilfield was calculated. Oil reservoirs were screened and classified on the basis of two types (suitable for immiscible displacement and not suitable for immiscible displacement). The classification results are given in Table 22 and Figure 61. The results show that 87 oil reservoirs in Yanchang Oilfield are suitable for immiscible displacement, accounting for 49 per cent of the total, and contribute to oil reserves of 1,147,337,500t, accounting for 53 per cent of the total of total reserves.

**Figure 61. Chart for classification of oil reservoirs with $CO_2$ immiscible displacement.**

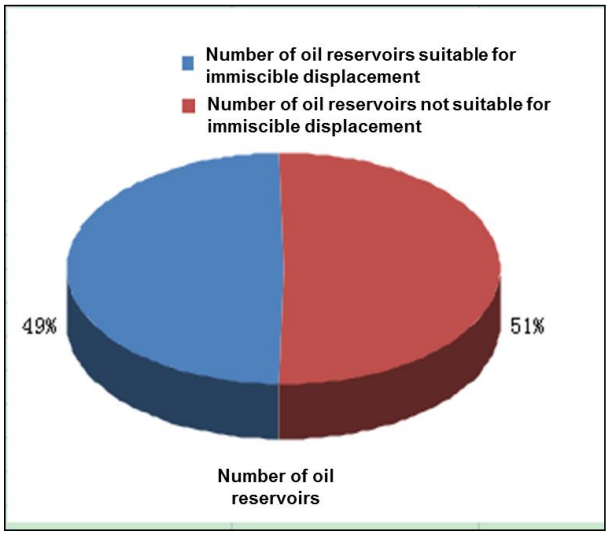


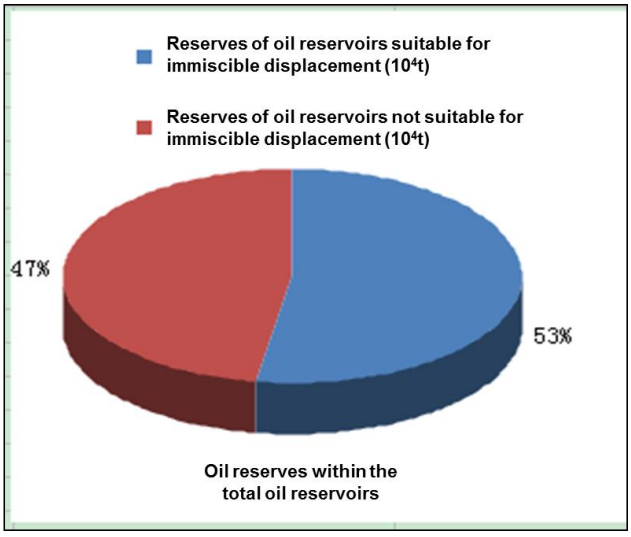


**Table 22. Screening results of oil reservoirs with $CO_2$ Immiscible displacement sequestration and enhanced oil recovery.**

| Total number of oil reservoirs | Number of oil reservoirs suitable for immiscible displacement | Proportion of oil reservoirs (%) | Total oil reserves (104t) | Oil reservoirs suitable for immiscible displacement (104t) | Proportion of reserves (%) |
|---|---|---|---|---|---|
| 176 | 87 | 0.49 | 218137.96 | 114733.75 | 0.53 |

## 7.2 Assessment results of sequestration potential of Yanchang Oilfield

The theoretical $CO_2$ sequestration capacity, effective $CO_2$ sequestration capacity, practical $CO_2$ sequestration capacity, EOR, $CO_2$ utilisation coefficient and $CO_2$ sequestration coefficient was estimated for the immiscible Yanchang oil fields. The $CO_2$ sequestration potential is based on the definitions of the CSLF (2007). The statistics and calculation indicate that:

- oil reservoirs suitable for immiscible displacement 1,256,902,100t
- theoretical capacity is 656,831,800t
- effective capacity is 394,093,100t
- practical capacity is 315,274,500t
- average EOR is 8.80 per cent
- average $CO_2$ utilisation coefficient is approximately 0.36
- average $CO_2$ sequestration coefficient is approximately 0.25.

Based on actual situation and data of the target block, the calculation of $CO_2$ sequestration capacity of two oil reservoirs (Wuqi-Yougou, Jingbian-Qiaojiawa) was made by $CO_2$ sequestration capacity calculation software. For calculation results, see Table 23.

**Table 23. Assessment Results of $CO_2$ sequestration potential of target reservoir in Yanchang Oilfield.**

| Oil Reservoir | | Geological Reserves (104t) | Practical Capacity (104t) | EOR (%) | $CO_2$ Utilisation Coefficient (Oil Increment per Ton of $CO_2$) | $CO_2$ Sequestration Coefficient (Decimal) |
|---|---|---|---|---|---|---|
| 1 | Jingbian-Qiaojiawa-Chang-6 | 931 | 209.87 | 4.03 | 0.18 | 0.23 |
| 2 | Wuqi-Yougou-Chang-4 & Chang-5 | 801 | 194.25 | 8.58 | 0.58 | 0.56 |

# 8 References

Carbon Sequestration Leadership Forum, 2007. Estimation of $CO_2$ storage capacity in geological media - phase 2, Washington DC: Carbon Sequestration Leadership Forum.

Celia, M.A., Bachu, S., Nordbotten, J.M., Kavetski, D., Gasda, S.E., 2005. Modeling Critical Leakage Pathways in a Risk Assessment Framework: Representation of Abandoned Wells. Conference Proceedings, Fourth Annual Conference on Carbon Capture and Sequestration DOE/NETL, May 2e5.

Global CCS Institute, 2016. Global Status of CCS: 2016.

Jenkins, C., Chadwick, Hovorka, S.D. 2015. The state of the art in monitoring and verification—Ten years on. International Journal of Greenhouse Gas Control, 40: 312–349.

Michelucci, D. and Faudot, D. 2005. A reliable curves tracing method. International Journal of Computer Science and Network Security 5: 10.

Shaanxi Yanchang Petroleum. 2015. CCS: A China Perspective Yanchang Petroleum Report 2: $CO_2$ storage and EOR in ultra-low permeability reservoir in the Yanchang Formation, Ordos Basin. Global CCS Institute Report, Melbourne.

## Acknowledgements

This report benefitted from the review and editing of the Global CCS Institute including Chris Consoli, Qianguo Lin, Antonios Papaspiropoulos and Jelena Susa.